Basin Research

IAS EAGE

Basin Research (2011) doi: 10.1111/j.1365-2117.2011.00511.x

Quantification and causes of the terrigeneous sediment budget at the scale of a continental margin: a new method applied to the Namibia–South Africa margin

F. Guillocheau,*,† D. Rouby,*,† C. Robin,*,† C. Helm,*,† N. Rolland,*,†,[1] C. Le Carlier de Veslud*,† and J. Braun‡,§

*Géosciences Rennes, Université de Rennes 1, Rennes Cedex, France
†CNRS/INSU, UMR 6118, Rennes Cedex, France
‡Laboratoire de Géodynamique des Chaînes Alpines, Université Joseph Fourier, Observatoire des Sciences de l'Univers de Grenoble, Grenoble Cedex, France
§CNRS/INSU, UMR 5025, Observatoire des Sciences de l'Univers de Grenoble, Grenoble Cedex, France

ABSTRACT

The terrigeneous sediment budget of passive margin basins records variations in continental relief triggered by either deformation or climate. Consequently, it becomes a major challenge to determine sediment accumulation histories in a large number of basins found in various geodynamic contexts. In this study, we developed a GIS-based method to determine the sediment budget at the scale of a whole basin (from the upstream continental onlap to the most distal deepest marine deposits) and the associated uncertainties. The volume of sediments preserved in the basin for each time interval was estimated by interpolation between cross-sections and then corrected from *in situ* production and porosity to obtain terrigeneous solid volumes. This approach was validated by applying it to Namibia–South African passive margin basins for which independent data are available. We determined by a statistical approach the variances associated with each parameter of the method: the geometrical extrapolation of the section (8–43%), the uncertainties on seismic velocities for the depth conversion (2–10%), on the absolute ages of stratigraphic horizons (0.2–12%), on the carbonate content (0.2–46%) and on remaining porosities estimation (3–5%). Our estimates of the accumulated volumes were validated by comparison with previous estimates at a lower temporal resolution in the same area. We discussed variations in accumulation rates observed in terms of relief variations triggered by climate and/or deformation. The high accumulation rates determined for the Lower Cretaceous, progressively decreasing to a minimum in the Mid-Cretaceous, are consistent with the progressive relaxation of a rift-related relief. The following increase to an Upper Cretaceous maximum is consistent with a major relief reorganization driven either by an uplift and/or a change to more humid climate conditions. The lower accumulation rate in the Cenozoic suggests a relief reorganization of lesser amplitude over that period.

INTRODUCTION

Products of continental erosion are commonly preserved in intra-continental and margin basins. The terrigeneous sediment budget preserved within these basins records variations in continental relief triggered by forcing factors such as deformation (e.g. an acceleration in rock uplift creates relief to be eroded, e.g. Selby, 1985; Duff, 1993; Moore, 1999) or climate (e.g. climatic changes alter the erosivity within the drainage area, and in doing so, affect the sediment supply reaching the basin; e.g. Bonnet & Crave, 2003). As a result, over geological time scales, the interpretation of sediment supply in terms of relief variations in the drainage area is far from straightforward. In this context, it is a major challenge to determine sediment accumulation histories in a large number of basins in various geodynamic contexts (both climatic and tectonic).

In order to determine these histories, the evolution of the whole sedimentary system should be integrated from the upstream onlap to the most distal deposits on the oceanic crust, in the case of passive margin basins, in order

Correspondence: D. Rouby, Géosciences Rennes, Université de Rennes 1, Campus de Beaulieu, 35042 Rennes Cedex, France. E-mail: delphine.rouby@univ-rennes1.fr
[1] Present address: CV Associés, Le Robinson, Rue Pelletier, 64200 Biarritz, France.

to incorporate the distribution of sediments across the basin (Fig. 1). Indeed, evaluations based on data sets located only within the proximal part of the basin (usually the shelf domain) will be biased by the transit of terrigeneous supply across the shelf down to the distal basin and might therefore significantly underestimate the accumulated amounts. Also, accumulation histories should be evaluated in areas large enough to incorporate sediment transport parallel to the margin, i.e. long-shore sediment transport. Within this perspective, the three-dimensional (3D) sediment budget at the scale of a whole basin has been successfully determined using different approaches combining isopach maps and well constraints (e.g. Poag & Sevon, 1989; Rust & Summerfield, 1990; Métivier *et al.*, 1999; Galloway, 2001; Clift *et al.*, 2002a, b; Jones *et al.*, 2002; Leturmy *et al.*, 2003; Walford *et al.*, 2005; Tinker *et al.*, 2008b; Rouby *et al.*, 2009). However, very few 3D data sets are available at the scale of a whole basin, not to mention a whole continent, as they usually only cover a few hundred square kilometres and are restricted to areas of economic interest.

Our objective was thus to develop a simple approach, that is easy to implement, in order to assess sediment accumulation histories at the basin scale using two-dimensional (2D) regional sections that have already been published for most of the basins worldwide. The major effort in this was to integrate heterogeneous data (e.g. seismic section, wells, maps, etc.) showing diverse qualities, spatial distributions and temporal resolutions. To carry this out, we used a GIS-based technique that compiled several 2D regional cross-sections in each studied basin. The volume of sediments accumulated in the basin for each time interval was estimated from the interpolation between the cross-sections. The novel aspect of our approach is that we integrated the whole domain in sedimentation (i.e. from the upstream onlap to the most distal deposits on the oceanic crust). We determined by a statistical approach the variances associated with each parameter of the method.

Our ultimate aim was to apply this method at the scale of a whole continent, namely Africa, for the entire Meso-Cenozoic period. With that future perspective in mind, the objective of this paper was to validate our approach in an area of the African continent for which independent data are available: i.e. the South Atlantic margin basins in Namibia and South Africa, which cover an area large enough to incorporate the redistribution of sediments both across and along the margin. This area is also of particular interest in terms of existing constraints on offshore accumulation and onshore denudation: (i) previous works have already quantified sedimentation rates at a very low temporal resolution (i.e. a scale of tens of Myr) using published isopach maps (e.g. Rust & Summerfield, 1990; Rouby *et al.*, 2009) and (ii) significant work has been carried out to determine the denudation history of the margin since rifting (from fission track analysis: Gallagher & Brown, 1999a, b; Brown *et al.*, 2002; Raab *et al.*, 2002, 2005; Kohn *et al.*, 2005; Tinker *et al.*, 2008a). These previous works have provided us with a very detailed framework within which we validated our multi-2D approach. Also among our primary objectives was the assessment of the associated uncertainties, which are as important as the accumulation values themselves.

METHODS FOR QUANTIFYING SEDIMENT BUDGET

Methods to determine volumes of sediment accumulation in 3D at the scale of a whole basin using subsurface data (combining isopach maps and well data) have already been successfully developed. Among the pioneer works, Poag & Sevon (1989) used a very complete subsurface data set collected along the United States middle Atlantic continental margin to establish isopach maps and, from this, a 3D sedimentary budget for time increments of a few Myr over the Meso-Cenozoic. Liu & Galloway (1993) and Galloway (2001) made higher resolution measurements along the

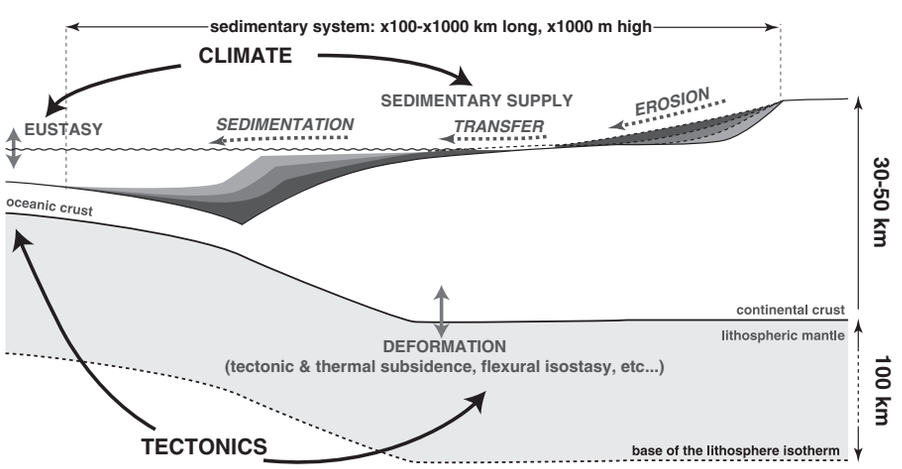

Fig. 1. Sketch of a margin sedimentary system defined from the drainage divide down to the distal most deposits onto the oceanic crust, i.e. including the areas both in erosion and sedimentation. Parameters influencing the transfer of sediments from one domain to another are shown: climate and tectonics, acting on deformation, eustasy and sediment supply.

Gulf of Mexico of the USA, that where however restricted to the most proximal parts of the margin (platform and delta front). A similar approach has been used for the Himalaya systems (Métivier *et al*., 1998, 1999) and associated basins (Métivier & Gaudemer, 1997, 1999; Clift *et al*., 2002a, b; Clift, 2006), also at time increments of a few Myr over the Cenozoic. The major limitation of this type of approach is the scarcity of isopach data available at the scale of the whole basin. When data are available, they are often restricted to the proximal parts of the margin (from the shelf to the toe of the slope).

For Africa, estimates of volumes of sediment accumulation in 3D have been carried out along the whole Namibia–South Africa margin at low resolution (four time increments in the Meso-Cenozoic; Dingle & Hendey, 1984; Rust & Summerfield, 1990; Rouby *et al*., 2009). Using petroleum exploration subsurface data, Leturmy *et al*. (2003) determined the 3D sediment budget of the Lower Congo Basin at a more detailed resolution (at time increments of a few Myr over the Meso-Cenozoic). Yet, most of the other estimates are restricted to the proximal part of the margin. For example, Walford *et al*. (2005) and Tinker *et al*. (2008b) established the 3D sediment budget of the Zambezi Delta and southern Cape offshore basins respectively, at a temporal resolution of a few million years. Finally, several authors estimated sediment accumulation from 2D sections usually restricted to the shelf domain and its toe at time increments of a few Myr over the Meso-Cenozoic (e.g. Lavier *et al*., 2001). As a consequence, estimates that detail sediment accumulation at high temporal resolution are usually limited to small sections of basins, whereas estimates for entire basins usually have very low temporal resolutions.

Accordingly, our objective was to develop and test a method that would allow us to evaluate sediment accumulation histories at the basin scale and integrate the whole domain in sedimentation (from the upstream onlap down to the most distal deposits). The method must be easy to implement in every type of basin (passive margin, intracontinental, etc.). We developed an approach method based on 2D regional sections available in most basins worldwide as well as a statistical approach to estimate associated uncertainties.

PRINCIPLE OF THE METHOD

The procedure remained the same regardless of the temporal resolution, which will depend on the data available for each basin. We first measured the total volume of accumulated sediments for each time interval by interpolation between cross-sections (Fig. 2). These were established from the extrapolation of published cross-sections that were usually limited to the most proximal part of the margin. The cross-sections were compiled to represent the variability of the stratigraphic architecture of the basin,

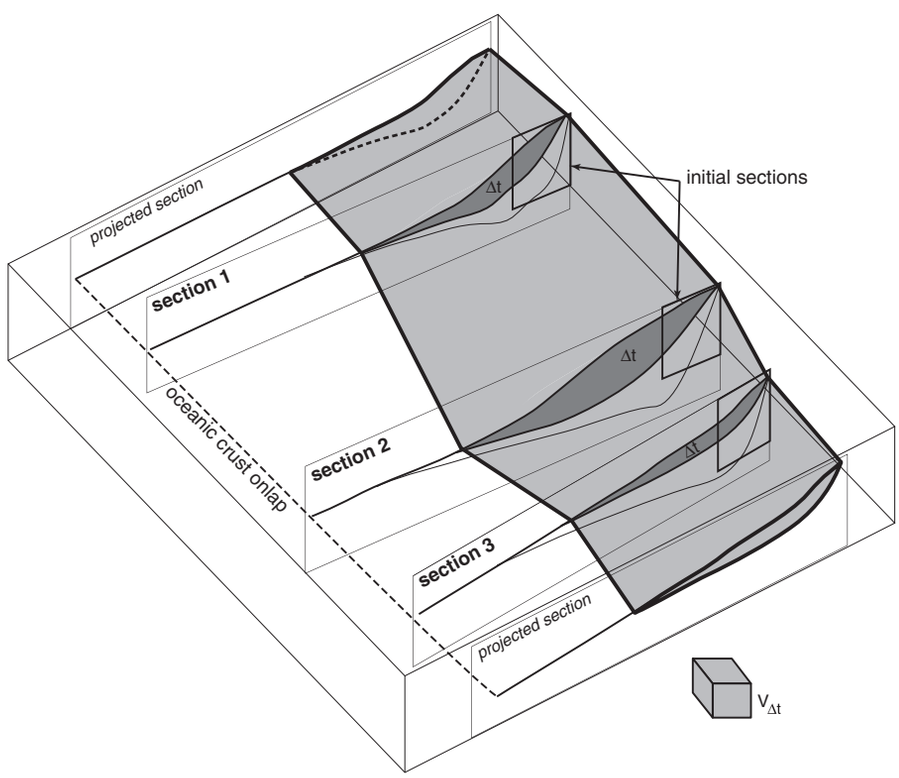

Fig. 2. Principle of the method. During the time interval Δt, the volume of sediments $V_{\Delta t}$ in the basin for each time interval is estimated by an interpolation between the cross-sections. The cross-sections are compiled to represent the variability of the stratigraphic architecture of the basin, and therefore are not necessarily regularly spaced (e.g. sampling of the main deltas and basement highs). They cover the whole sedimentary wedge from the onshore onlap down to the most distal deposits over the oceanic crust.

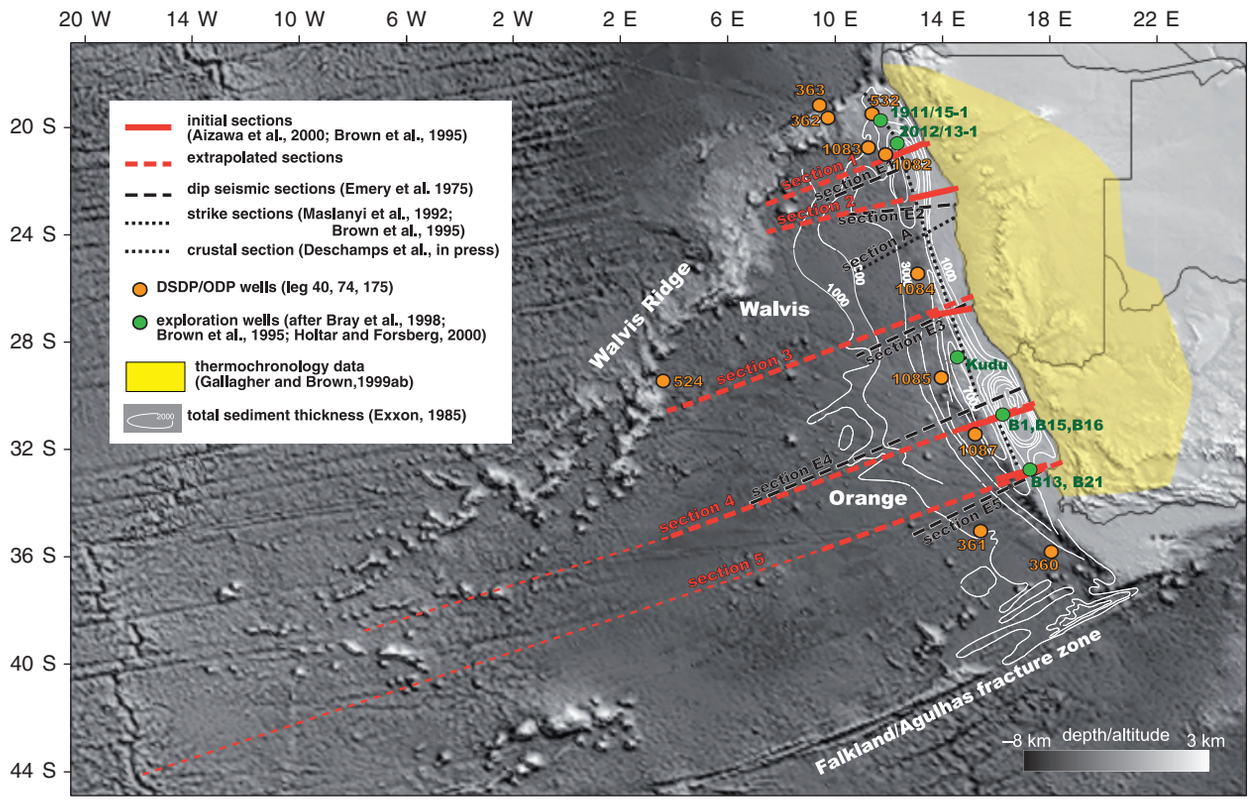

Fig. 3. Location of the studied area and data used to constrain the geometry of the sedimentary wedge. The topography and bathymetry are shown in the shaded grey scale (source Etopo2). The contour lines of the offshore total sedimentary thickness (after Exxon, 1985) are shown in white. The location of the cross-sections built for this example, the initial cross-sections and some of the sections available in the literature are shown as dashed red lines, a thick black line and a dashed white line, respectively (after Emery *et al.*, 1975; Maslanyj *et al.*, 1992; Brown *et al.*, 1995; Deschamps *et al.*, in press). The location of the ODP/DSDP wells (Bolli *et al.*, 1978; Moore *et al.*, 1984; Wefer *et al.*, 1998) is shown as white dots and exploration wells as black dots (McMillan, 1990, 2003; Wickens & McLachlan, 1990; Brown *et al.*, 1995; Bray *et al.*, 1998; Holtar & Forsberg, 2000). The coverage of thermochronology data is shown in the yellow-shaded area (after Gallagher & Brown, 1999a, b).

and thus were not necessarily regularly spaced (e.g., sampling of the main deltas and basement highs). The cross-sections were integrated into a GIS database to allow for the harmonization of the geographical projections and quantification of the geometric dimensions. For each time interval for each section, the mean deposited thickness and rate of deposition were estimated. Then the area of deposition was determined by an interpolation between the cross-sections. The product of the mean deposited thickness and area of deposition gave the volume accumulated in the basin for each time interval.

This volume included the particulate supply resulting from mechanical erosion regardless of its transport mode (wind/flood) as well as the *in situ* production (e.g. carbonates, volcano-clastics, volcanics). This also included the porosity remaining after the sediments underwent partial compaction since their deposition (older accumulation volumes and rate are less biased by porosity than the younger ones). In order to use these volumes in terms of a 'source to sink' analysis, i.e. to discuss the variations of continental relief producing the sediments reaching the basin, both the *in situ* production and remaining porosity must be estimated and the total volumes corrected in order to obtain terrigeneous solid volumes. The latter may then be compared to rock volumes eroded on the continent (e.g. estimated by thermochronology). However, these volumes do not include the dissolved part of the erosion, which also contributes to the continental denudation (chemical weathering).

GEOLOGICAL SETTINGS

The studied area included the basins of the Namibian/South African passive margin located between the Walvis Ridge and Falkland–Aghulas fracture zone, i.e. the Walvis, Luderitz and Orange Basins (Fig. 3). For the sake of simplicity, we will refer to both the Luderitz and Orange Basins as 'Orange Basin' for the remainder of this work. The basins of this margin are filled by a thick sedimentary wedge showing two main depocentres (i.e. the Walvis and Orange basins), locally reaching 8 km in thickness and thinning out seaward over 800–1000 km (Figs 3 and 4a).

Syn-rift evolution

The onset of the rift that led to the formation of this margin, as well as the exact geometry and extent of the syn-rift

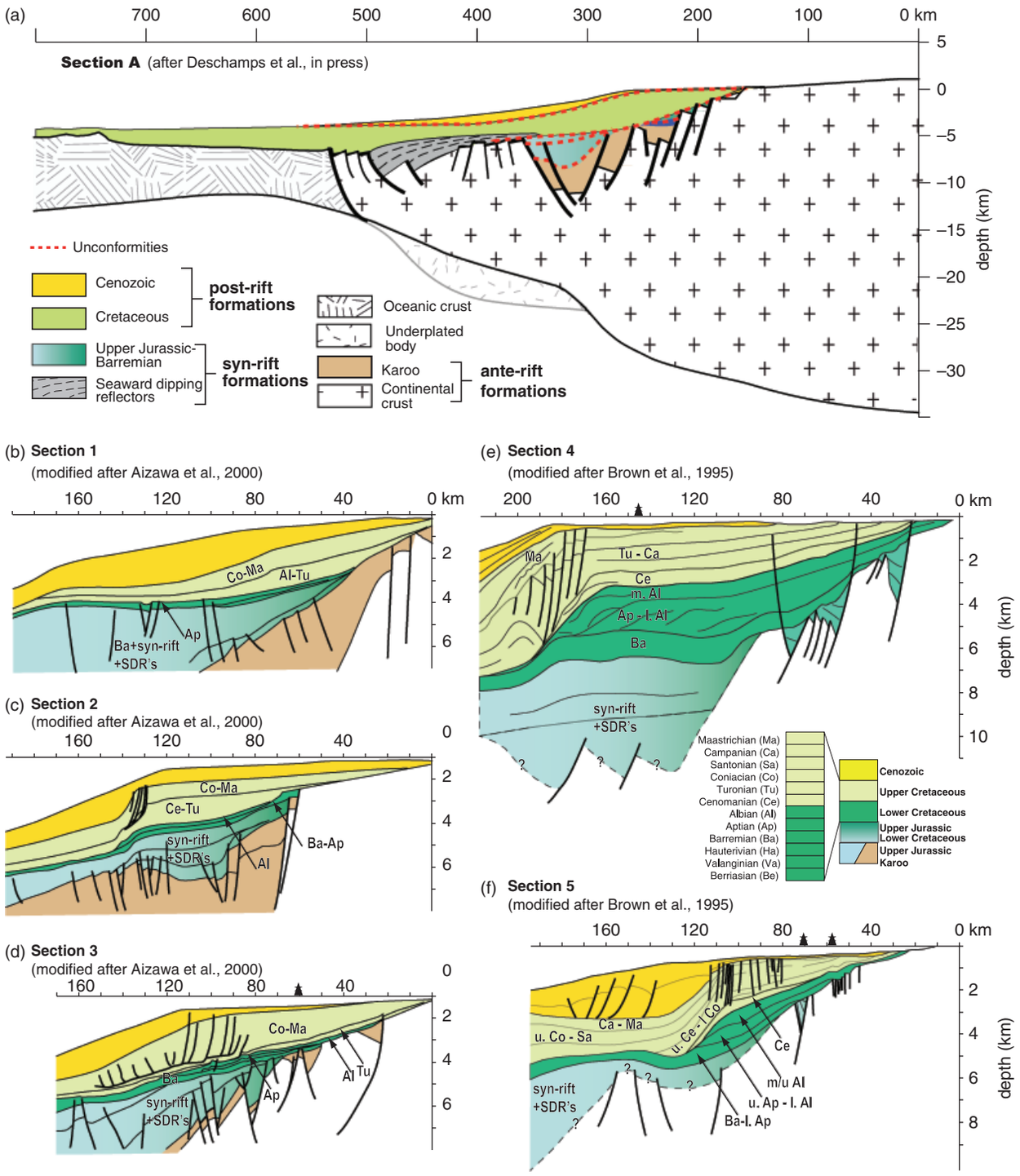

Fig. 4. (a) Synthetic section of the Namibian margin at the crustal scale [after Deschamps *et al.* (in press); established after Smith & Sandwell (1997) for the topography and bathymetry; Artemieva & Mooney (2001) for the crustal thickness; Emery & Uchupi (1984) for the sedimentary wedge thickness; Light *et al.* (1993); Gladczenko *et al.* (1998); Bauer *et al.* (2000); Trumbull *et al.* (2002) for the sedimentary wedge geometry]. (b–d) Initial sections published by Aizawa *et al.* (2000) modified after Maslanyj *et al.* (1992), Light *et al.* (1993), Holtar & Forsberg (2000). (e, f) Sections 4 and 5 by Brown *et al.* (1995) modified after Paton *et al.* (2007, 2008), Hirsch *et al.* (2010). See Fig. 3 for locations.

sequences, are not yet fully constrained. It is generally acknowledged, by analogy with the Gamtoos and Algoa Basins where it is well dated (McMillan, 1990; Paton *et al.*, 2008), that the rifting occurred during the late Upper Jurassic (i.e. about 155 Myr) and then propagated northward from the Falkland–Aghulas fracture zone to the Walvis Ridge (see the review in Jackson *et al.*, 2000 for example). However, along the Namibian margin, Light *et al.* (1993)

proposed that the rifting actually occurred in two episodes: one ending in the Valanginian (136 Myr) and another ending in the Hauterivian (140 Myr). Alternatively, rift structures predating the Late Jurassic–Early Cretaceous Atlantic rift have been described in the same area (most likely of Karoo age i.e. Permo-Triassic; Clemson *et al.*, 1997, 1999; Aizawa *et al.*, 2000; Corner *et al.*, 2002).

The rift basins (Fig. 4a) are filled by siliciclastic, fluvial and deltaic series (e.g. Gerrard & Smith, 1982; Light *et al.*, 1993; Van der Spuy, 2003; Hirsch *et al.*, 2010). In addition, the margin is characterized by significant volcanic activity during the rifting (e.g. Gladczenko *et al.*, 1997, 1998; Bauer *et al.*, 2000; Corner *et al.*, 2002; Fernandez *et al.*, 2010). Evidence of seaward dipping reflectors (SDR: sub-aerial volcanic flow emplaced during rifting; Fig. 4a) and well data indicate that the syn-rift geometries along both the Namibian and South African margins also include significant, but unknown, amounts of volcanic and volcano-clastic deposits (e.g. Gerrard & Smith, 1982; Light *et al.*, 1993; Gladczenko *et al.*, 1998; Bauer *et al.*, 2000; Jackson *et al.*, 2000; Mohriak *et al.*, 2002; Van Der Spuy, 2003; Hirsch *et al.*, 2010).

Post-rift evolution

In contrast, the drift onset is fairly well constrained. The age of the break-up is generally acknowledged to have occurred at the end of the Hauterivian in the Orange Basin (about 130 Myr; e.g. Brown *et al.*, 1995, based on biostratigraphic data from McMillan, 2003) and assumed to be of the same age in the Walvis Basin (Gerrard & Smith, 1982; Maslanyj *et al.*, 1992; Light *et al.*, 1993). The post-rift sedimentary sequence (Fig. 4a) is a thick wedge, mostly siliciclastic, of open marine environment (e.g. Dingle *et al.*, 1983; Brown *et al.*, 1995). It has aggraded (and slightly prograded) over most of the Cretaceous (130–65 Myr) and shifted seaward during a period of time from the latest Cretaceous to the early Cenozoic (65 Myr–present; e.g. Dingle *et al.*, 1983; Light *et al.*, 1993; Brown *et al.*, 1995; Stevenson & McMillan, 2004; Paton *et al.*, 2008).

Evolution of the Namibia–South Africa margin relief

The domain in erosion currently feeding the Namibia–South Africa passive margin is the western rim of the southern African plateau. The present day drainage shows three domains (Fig. 3): (i) a low relief and a high average elevation plateau (>1000 m) bounded by (ii) high relief zones (i.e. steep escarpment faces) separating it from the coastline and (iii) a low relief and low elevation coastal plains. It is generally acknowledged that the large catchment of the Orange River, covering most of South Africa, has been acquired during the Upper Cretaceous (Proto-Orange; e.g. De Wit *et al.*, 2000; Goudie, 2005) or even in the late Early Cretaceous (mid-Albian; Stevenson & McMillan, 2004).

On the other hand, the origin and age of the southern African plateau are highly debated. The very long wavelength of the anomaly ($\times$ 1000 km) suggests a deep origin (Nyblade & Robinson, 1994), potentially related to a mantle anomaly that has been characterized by seismic tomography below the current position of southern Africa (e.g. Ni *et al.*, 1999; Ritsema *et al.*, 1999; Gurnis *et al.*, 2000; Nyblade *et al.*, 2000; Ritsema & Van Heijst, 2000; Ni *et al.*, 2002). A wide range of hypotheses have been proposed for the age of the uplift: for example, over the Mesozoic (Pysklywec & Mitrovica, 1999; van der Beek *et al.*, 2002; Nyblade & Sleep, 2003); in the Jurassic at the time of the emplacement of the Karoo volcanics (Cox, 1989); in the late Cretaceous (Gallagher & Brown, 1999a, b; de Wit, 2007; Tinker *et al.*, 2008a, b); or in the late Cenozoic ($\sim$30 Myr, Burke, 1996; Burke & Gunnell, 2008; $\sim$3 Myr, Partridge & Maud, 1987). Palaeotopographic reconstructions based on cooling histories (Gallagher & Brown, 1999b) suggest that the Namibia–South Africa margin has displayed a fairly important relief (reaching at least 2 km) since at least 100 Myr.

DATA SET AND INITIAL CROSS-SECTIONS

Principle

The first step of the method was to compile the data available for the studied basin in the literature (e.g. cross-sections, DSDP/ODP/IODP reports, published wells, etc.) in order to establish coherence among them in terms of the (i) horizontal and vertical scale, (ii) chronostratigraphic subdivisions and (iii) lithology.

(i) As already pointed out, published cross-sections are usually limited to the shallowest part of the basin (shelf and proximal slope). Initial cross-sections were chosen among them to represent the variability of the geometry of the basin. Depending on the data available, we attempted to sample the main depocentres and basement highs; sections are typically a few hundred kilometres apart and not necessarily evenly spaced. When published cross-sections were available only in two-way travel time rather than in depth, we performed a depth conversion using seismic velocities provided either by the authors or, most commonly, in publications for the same basin or area. We usually assumed a homogeneous velocity between the seismic markers and we tested several velocity models in order to estimate the associated uncertainties. Initial cross-sections were then brought into a GIS database in order to harmonize the geometrical dimensions.

(ii) The stratigraphic resolution of the initial cross-sections also defines the stratigraphic resolution of the extrapolated sections and, in doing so, the temporal resolution of the sediment accumulation measurements. In a first step, we re-evaluated the stratigraphic age of every stratigraphic surface and sediment wedge using data that was published afterwards. We then calibrated these re-evaluated stratigraphic ages in absolute ages using the ICS (2004) stratigraphic chart. We

took into account uncertainties associated with these absolute ages and quantified the variance of our results associated with it.

(iii) For each time interval, we estimated a mean lithology (percentages of sand, shale and carbonate). Again, the lithological description of the initial cross-sections will define the resolution of the lithological information for the extrapolated section. Most commonly, only local well data and synthetic lithostratigraphic charts for the whole basin are available. These estimations were later used to correct from the carbonate content and from the remaining porosity to finally obtain a terrigeneous solid accumulated volume.

Application to the Namibia–South Africa margin

Five initial cross-sections were chosen for the Namibia–South Africa margin: two in the Walvis Basin, and three in Orange Basin (Figs 3 and 4; Table 1). We depth converted three of the sections available only in two-way travel time (Tables 1 and 2; details in 'Uncertainties in seismic velocities'). Available well data were mostly located on the shelf, at its toe, and on the shallow Walvis Ridge, whereas the distal plain was only sampled at the southern tip of the Orange Basin (Table 1).

The extensive exploration of the Orange–Walvis Basin has allowed for a very good stratigraphic description of the Cretaceous formations (e.g. seismic stratigraphy: Brown *et al.*, 1995 based on the biostratigraphy of foraminifera provided by McMillan, 2003). For the Walvis Basin, no biostratigraphic data have been published. Thus, we used the stratigraphic ages provided by Aizawa *et al.* (2000), with the exception of the seismic lines published by Emery *et al.* (1975), for which we re-evaluated the age of the stratigraphic surfaces [see details in 'Extrapolation of section 2 (Walvis Basin)']. Every time line was then recalibrated to the ICS (2004) stratigraphic chart.

The resulting stratigraphic resolutions of the initial cross-sections are therefore variable (Fig. 4): it is poorly calibrated for the syn-rift (see 'Syn-rift evolution'), yet well determined for the Cretaceous (the resolution falls within the range of the stratigraphic stage i.e. a few Myrs). Furthermore, the Cenozoic is represented by a single time-interval because of the lack of intra-Cenozoic dating available in the literature. Also, the boundaries of the time intervals vary from one section to another.

EXTRAPOLATED CROSS-SECTIONS AND ASSOCIATED UNCERTAINTIES

Principle

As currently published cross-sections are usually restricted to the most proximal part of the margin (i.e. the shelf and its toe), the second step of our method was to extrapolate the initial sections over the entire sedimentary wedge (from the upstream onlap down to the most distal deposits over the oceanic crust; Fig. 5) using available geological data: (i) low resolution isopach maps, (ii) academic seismic surveys, (iii) DSDP/ODP/IODP and exploration wells and (iv) the age of the oceanic crust, in order to constrain the distal geometry of the sedimentary wedge at each time interval. This extrapolation step was also based on basic stratigraphic concepts of the architecture of sedimentary systems: the shelf and slope behaviour (prograding, aggrading or retrograding trend) was used to constrain the geometry of the deep-sea wedge (volumetric partitioning implies condensation in the distal parts during retrogradation and deep-sea fans during forced regression). This allowed us to restrict the extrapolation to only stratigraphically consistent hypotheses.

We then attributed a confidence value (probability in percent) to each extrapolation hypothesis based on the knowledge of the margin geology (e.g. structure, deformation history, main eustatic events). The preferred scenario is merely the most probable scenario in terms of sequence stratigraphic concepts, which should not be used without associated uncertainties. Figure 5 illustrates this procedure using a theoretical example. In extrapolation 1 (Fig. 5c), the sedimentary wedge deposited during time interval Δt_1 onlaps the oceanic crust (maximum extent of the sedimentary wedge scenario). In extrapolation 2, it downlaps older deposits at the toe of the slope (minimum extent scenario). Extrapolation 3 illustrates a case involving the erosion of the wedge after it was deposited during the time interval Δt_3. In this case, the initial geometry of the wedge is reconstructed to estimate the actual deposited geometry (Fig. 5d). Other sources of uncertainties are discussed below ('Resolution and source of uncertainties').

Extrapolation of section 2 (Walvis Basin)

The extrapolation procedure for section 2 is detailed in Figs 6 and 7. The initial cross-section 2 (Fig. 4c; Table 1) has been modified using available data (i.e. Maslanyj *et al.*, 1992; Light *et al.*, 1993; Clemson *et al.*, 1999; Holtar & Forsberg, 2000) and well data (ODP leg 175 sites 1082–1084 that do not reach sediments older than the late Miocene; Table 1; Wefer *et al.*, 1998). In the Walvis Basin, the main uncertainty is the geometry and age of the syn-rift deposits (especially at the base), as well as the ability to discriminate them from the Karoo (Triassic) rift sediments. We thus assumed a late Upper Jurassic age for the syn-rift deposits by analogy with the Orange Basin. Based on well data (e.g. Holtar & Forsberg, 2000), we assumed an Albian age for the thin wedge at the base of the Albian-Turonian, which is only preserved on the shelf (Fig. 6e). Five main stratigraphic units have been defined accordingly on the initial section (see details in Fig. 6b).

To extrapolate shelf and slope geometries toward the abyssal plain, we used the framework of the total thickness of Meso-Cenozoic sediments mapped by Emery & Uchupi (1984; Fig. 6d) as well as the seismic line from Emery

Table 1. Data set compiled for the Orange–Walvis Basin

Data type	Label on Fig. 3	Location	Maximum age	Source
Sections				
Initial dip sections	Initial Section 1	Shelf	Lower Cretaceous	Aizawa *et al.* (2000)
	Initial Section 2			*TWT seismic section*
	Initial Section 3			(depth conversion using Emery *et al.*, 1975)
	Initial Section 4	Shelf	Lower Cretaceous	Brown *et al.* (1995), Paton *et al.*, (2007)
	Initial Section 5			Brown *et al.* (1995)
Other dip sections	Section E1	Shelf	Lower Cretaceous	Emery & Uchupi (1984)
	Section E2			
	Section E3			
	Section E4			
	Section E5			
Other strike sections	Section S1	Shelf	Lower Cretaceous	Maslanyj *et al.* (1992)
	Section S2			Brown *et al.* (1995)
Wells				
Exploration well	B1	Shelf	Lower Cretaceous	Brown *et al.* (1995)
	B13			
	B15			
	B16			
	B21			
	Kudu			McMillan (1990)
	2010/13-12			Bray *et al.* (1998)
	1911/15-1			Holtar & Forsberg (2000)
ODP Leg 175	1081	Deep sea plain	Upper Miocene–Pliocene	Wefer *et al.* (1998)
	1082			
	1083			
	1084			
	1085			
	1086			
	1087			
DSDP Leg 40	360	Distal plain	Cenozoic	Bolli *et al.* (1978)
	361		Lower Cretaceous	
	362	Shallow ridge	Cenozoic	Bolli *et al.* (1978)
	363		Lower Cretaceous	
DSDP Leg 74	524	Shallow ridge	Uppermost Cretaceous	Moore *et al.* (1984)
	532	Shelf	Upper Miocene–Pliocene	Moore *et al.* (1984)

Table 2. Seismic velocities (after Emery *et al.*, 1975) used for the depth conversion of the initial sections 1–3 (see Fig. 4)

Interval	Seismic velocity ($m\,s^{-1}$)					Uncertainties (%)
	Section 1	Section 2		Section 3		
	Proximal	Distal	Proximal	Distal		
Water	1500	1500	1500	1500	1500	–
Cenozoic	1600	2000	1600	2200	1700	7
Cretaceous	2100	2600	1900	3000	2400	10
Syn-rift+SDRs	3600	3500	3500	3700	3600	13
Basement	5400	5400	5400	5400	5400	–

SDR, seaward dipping reflectors.

et al. (1975) imaging the whole sedimentary wedge (Fig. 6c). We, however, re-evaluated the ages proposed by these authors for discontinuities AII and D (base Cenozoic and base Neogene, respectively) using data from wells that are now available (Gerrard & Smith, 1982; Light *et al.*, 1993; Brown *et al.*, 1995; Aizawa *et al.*, 2000; Paton *et al.*, 2007, 2008). On this section, more recent data (Gerrard & Smith, 1982; Light *et al.*, 1993; Brown *et al.*, 1995; Aizawa *et al.*, 2000; Paton *et al.*, 2007, 2008) suggest that the D discontinuity corresponds to the Cenozoic base (65 Myr) and AII discon-

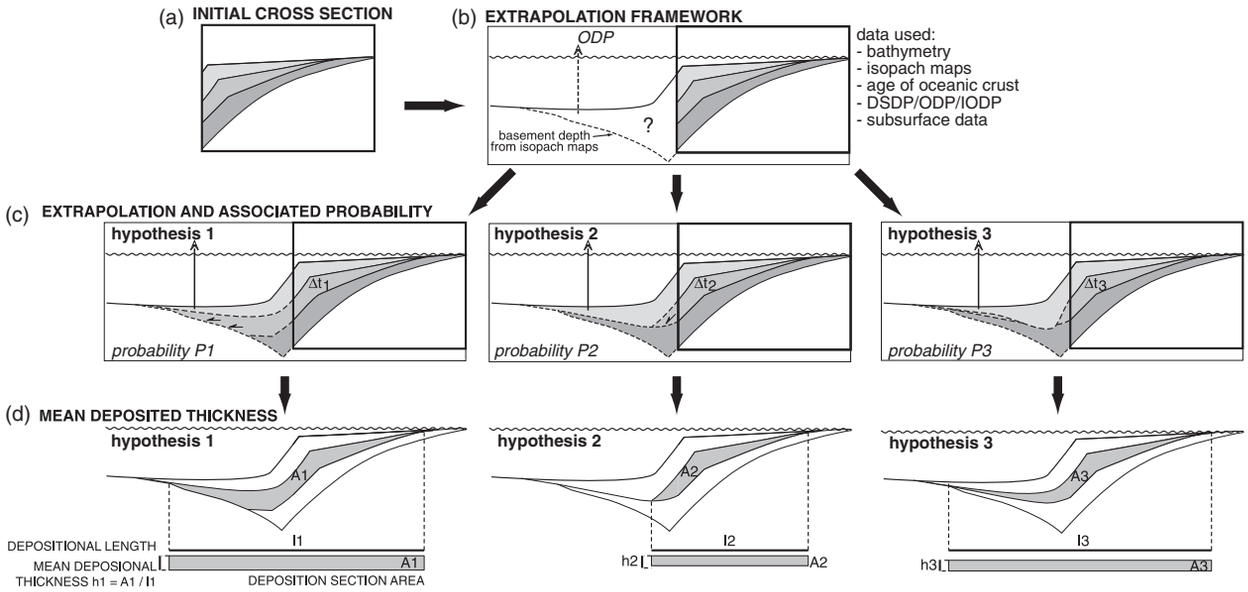

Fig. 5. Extrapolation method for the initial cross-sections and measurement of the mean deposited thickness for each time interval. (a) The initial cross-section is (b) extrapolated across the whole sedimentary wedge using all available data (e.g. bathymetry, ODP wells, total isopach maps, subsurface data, etc.; see text for details). (c) For each initial section, several hypotheses are established within this extrapolation framework; three, in this case. See text for details. (d) For each hypothesis and time interval Δt_i, the mean deposition length l_i and deposited section area A_i are measured. The mean deposited thickness h_i is then deduced as $h_i = A_i/l_i$.

tinuity to a major discontinuity, either of late Upper Cretaceous age (base Coniacian – 89 Myr) or Lower Cretaceous age (base Barremian – 130 Myr). Four seismic units have been accordingly defined (see details in Fig. 6c).

We tested four extrapolation hypotheses for section 2 to evaluate uncertainties related to both (i) the geometry of the sedimentary wedge in the distal part of the basin and (ii) the age attributed to unconstrained stratigraphic markers (Fig. 7). The total sediment thickness (Emery & Uchupi, 1984; Fig. 6d) shows a significant thickening below the present-day slope which is in good agreement with the thickening of the syn-rift on the initial cross-section published by Aizawa *et al.* (2000), although located slightly seaward. Therefore, in our extrapolations of section 2 (Fig. 7e), syn-rift deposits are significantly thicker than initially suggested by Aizawa *et al.* (2000; Fig. 4c). This is more consistent with the thick syn-rift wedge shown by sections 1 and 3 (Fig. 4b and d). Also, crustal scale seismic data available along the Namibian Margin show seaward-dipping reflectors more than 500 km off the present day coastline (e.g. Gladczenko *et al.*, 1997, 1998; Bauer *et al.*, 2000; Corner *et al.*, 2002; Fernandez *et al.*, 2010;Fig. 4a). Consequently, in hypotheses 2a and 2b (Fig. 7), we assumed the occurrence of syn-rift sediments 300 km off the present-day coastline. However, we defined the geometry of these potential distal syn-rift deposits based the total thickness isopach (i.e. pinching seaward; Fig. 6d), which is thinner than the one shown in the crustal scale sections (i.e. thickening seaward; Fig. 4a; e.g. Gladczenko *et al.*, 1997, 1998). Also, discontinuity AII is assumed to be Barremian in age (early drift – 130 Myr) in hypotheses 2a and 2b and early Upper Cretaceous (base Coniacian – 89 Myr) in hypotheses 2c and 2d. Finally, seismic data provided by Corner *et al.* (2002) suggest clinoform geometries on the shelf during the Turonian. Consequently, in hypotheses 2a and 2c, the distal part of the progradational unit is draping seaward, whereas in hypotheses 2b and 2d, it downlaps at the toe of the shelf. We attributed a probability to each extrapolation hypothesis (2a: 45%; 2b: 35%; 2c: 5%; 2d: 15%; Fig. 7).

Geometry of the sedimentary wedge of the Namibia–South Africa margin

The compilation of the extrapolated sections provides a new description of the stratigraphic architecture of the whole Meso-Cenozoic sedimentary wedge at the scale of the Namibia - South Africa margin. Although Fig. 8 illustrates only the favoured extrapolation hypotheses of the five extrapolated sections, the following description is nonetheless relevant for all extrapolation hypotheses. Also, as the geometry of syn-rift deposits is not well constrained, it is not detailed here.

The whole wedge shows a first-order stratigraphic evolution consistent along-strike the margin, with however significant spatial variability in terms of preserved thicknesses. The Aptian to Turonian sedimentary wedge is thin and progressively restricted to the shelf with an overall retrograding trend. It is significantly dilated in the centre of the Orange Basin (south of the present day Orange River mouth; section 4 on Fig. 8). The Upper Cretaceous wedge forms the first major progradational unit of the margin with a main depocentre located at the toe of the shelf and

south of the present day Orange River mouth (section 4 on Fig. 8). The Cenozoic wedge, which also forms a prograding unit, follows it. It is however thinner than the Upper Cretaceous one and is different in that it shows depocentres in the northern and southern parts of the basin (sections 1, 2 and 5 on Fig. 8).

MEAN DEPOSITED THICKNESS FOR EACH TIME INTERVAL

The following step was used to determine the mean deposited thickness for each time interval Δt along each extrapolated cross-section (and for each hypothesis).

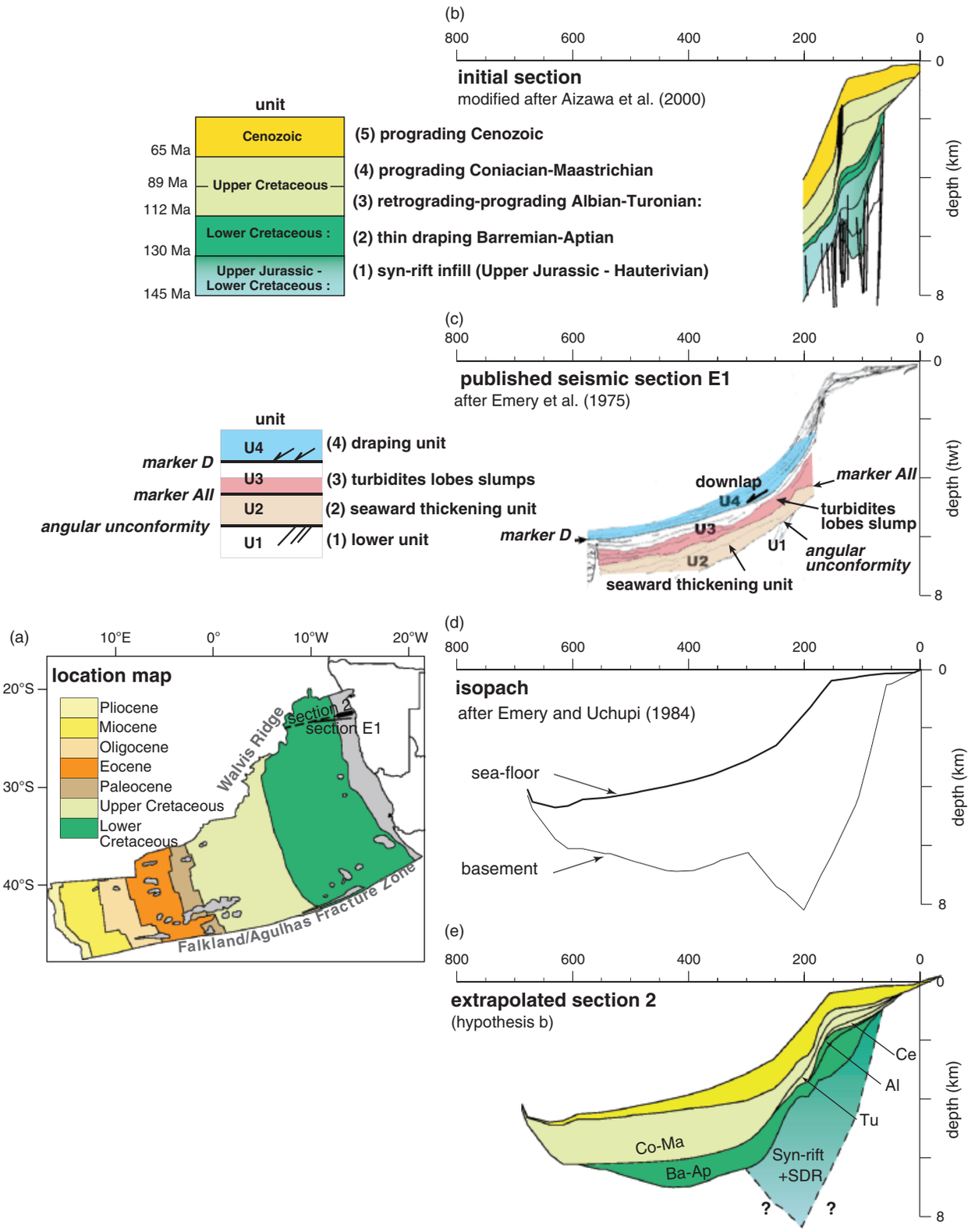

To do this, we measured the length of each sedimentary wedge (l_i in Fig. 5d). For the sake of simplicity, this curvilinear length along the depositional profile was approximated by its horizontal component, assuming that the slope of the sedimentary systems at that scale is negligible (e.g. a depositional profile reaches a maximum of a thousand metres high for a length of several hundreds of kilometres). We then measured the section area of the deposited wedge (A_i in Fig. 5d) and deduced the mean deposited thickness h_i ($h_i = A_i/l_i$). The difference between the various extrapolation hypotheses gave the uncertainty on the mean deposited thickness related to extrapolation and the age of unconstrained stratigraphic markers.

We only detail the results for section 2 (Table 3). For each extrapolation hypothesis, we show accumulation rates (mean deposited thickness h_i vs. time; Fig. 7c). Irrespective of the hypothesis, the accumulation rates decreased during the Lower Cretaceous (until the Albian, about 100 Myr), increased significantly in the lower Upper Cretaceous (with a peak in the Turonian, about 90 Myr) and decreased again in the late Upper Cretaceous and Cenozoic. The variability among the hypotheses lies mostly in the intensity of the Upper Cretaceous peak (ranging between 40 and 115 m Myr^{-1}).

Figure 9 shows the 2D accumulation rates determined for the five extrapolated sections. As pointed out earlier, the time increments vary from one section to another at this stage of the procedure: two to four increments for the Lower Cretaceous, one to three for the Upper Cretaceous and one step for the Cenozoic. Accumulation rates along the margin show a similar trend (Fig. 9; Table 4): they decreased during the Lower Cretaceous, increased significantly in the lower Upper Cretaceous and decreased again in the late Upper Cretaceous and Cenozoic. The variability between the hypotheses lies in the initial syn-rift sedimentation rate (ranging between 40 and 115 m Myr^{-1}) and in the intensity of the Upper Cretaceous peak (ranging from about 20 to 115 m Myr^{-1}). Nevertheless, the northern domain (sections 1–3) shows much lower accumulation rates during the post-rift Cretaceous than the southern domain (sections 4 and 5). This is associated with both the thick Lower Cretaceous and Cenomanian wedges preserved on the platform and the following Upper Cretaceous thick prograding wedges (sections 4 and 5; Fig. 8).

DEPOSITION AREA FOR EACH TIME INTERVAL

In order to convert these 2D accumulation rates into volumes, we first needed to map the horizontal area upon which deposition occurred (deposition area $D_{\Delta t}$; Fig. 10) for each time interval Δt for all sections. The maximum extent of the deposited wedge for each cross-section was therefore mapped by its projection onto a horizontal plane. It was then interpolated linearly between the sections (and projected from the edge sections onto the limits of the studied area; Fig. 10). This defined a polygon of deposition whose area can be measured (light grey area in Fig. 10). The difference in area between the various extrapolation hypotheses gives the uncertainty on the deposition area (dark grey area in Fig. 10).

Figure 11 and Table 5 show the temporal evolution of the mean deposition area (and associated uncertainties). The areas vary from about 0.2×10^{12} m^2 in the Albo-Cenomanian (106.8–93.5 Myr) to over 1.8×10^{12} m^2 for the Cenozoic basin extension (65.5–0 Myr): the size of the deposition basin actually increased significantly in the Campanian (about 80 Myr ago; Fig. 11b and c).

ACCUMULATED VOLUME FOR EACH TIME INTERVAL

At this stage, we estimated the volume of sediment accumulated during each time interval Δt, assuming a linear interpolation of the deposited thicknesses between the cross-sections (Fig. 12). To do this, the deposition area was subdivided into elementary polygons bounded by the cross-sections. The volume of sediments deposited in each polygon (V_i) was determined from its area (D_i) and the interpolated deposited thickness between the bounding cross-sections. The total volume of sediment deposited for the time interval $V_{\Delta t}$ is the sum of these elementary volumes.

These raw volumes were then corrected from *in situ* production (carbonates and volcanics) and from remaining porosity to reach solid terrigeneous volumes. We also evaluated the correction related to post-depositional sediment redistribution and to the long-shore transport.

Fig. 6. Extrapolation framework for section 2. (a) Location of the initial (thick black line) and extrapolated (dashed lines) sections and age of the oceanic floor (after UNESCO *et al.*, 1990). (b) Initial section modified after Aizawa *et al.* (2000). Above the Karoo rift deposits (Early to Middle Triassic age; Clemson *et al.*, 1999), there are five main stratigraphic units: (1) a syn-rift infill ending at the end of the Hauterivian (130 Myr), (2) a thin draping Barremian-Aptian unit (130–112 Myr), (3) a retrograding-prograding Albian-Turonian unit (112–89 Myr), (4) a prograding Coniacian-Maastrichtian unit (89–65 Ma) and (5) a stratigraphically undifferentiated prograding Cenozoic unit (65–0 Myr). (c) Line drawing of the seismic reflexion section E1 [modified after Emery *et al.*, 1975, see location in (a)]. It shows four units: (1) a lower unit, bounded on top by an angular unconformity of unknown age, (2) a thickening seaward unit, bounded on top by the AII discontinuity, (3) a continuous unit, showing evidence of mound-like structures, possibly corresponding to turbidity lobes and/or large slumps, bounded on top by the D discontinuity and (4) a progradational unit with dowlaps in the early phase of growing. The relationship between units 2 and 4 and the shelf is not shown on the section. (d) Total sedimentary wedge thickness after Emery & Uchupi (1984) showing a significant thickening below the present-day slope. (e) Extrapolation hypothesis b for section 2 (see Fig. 7).

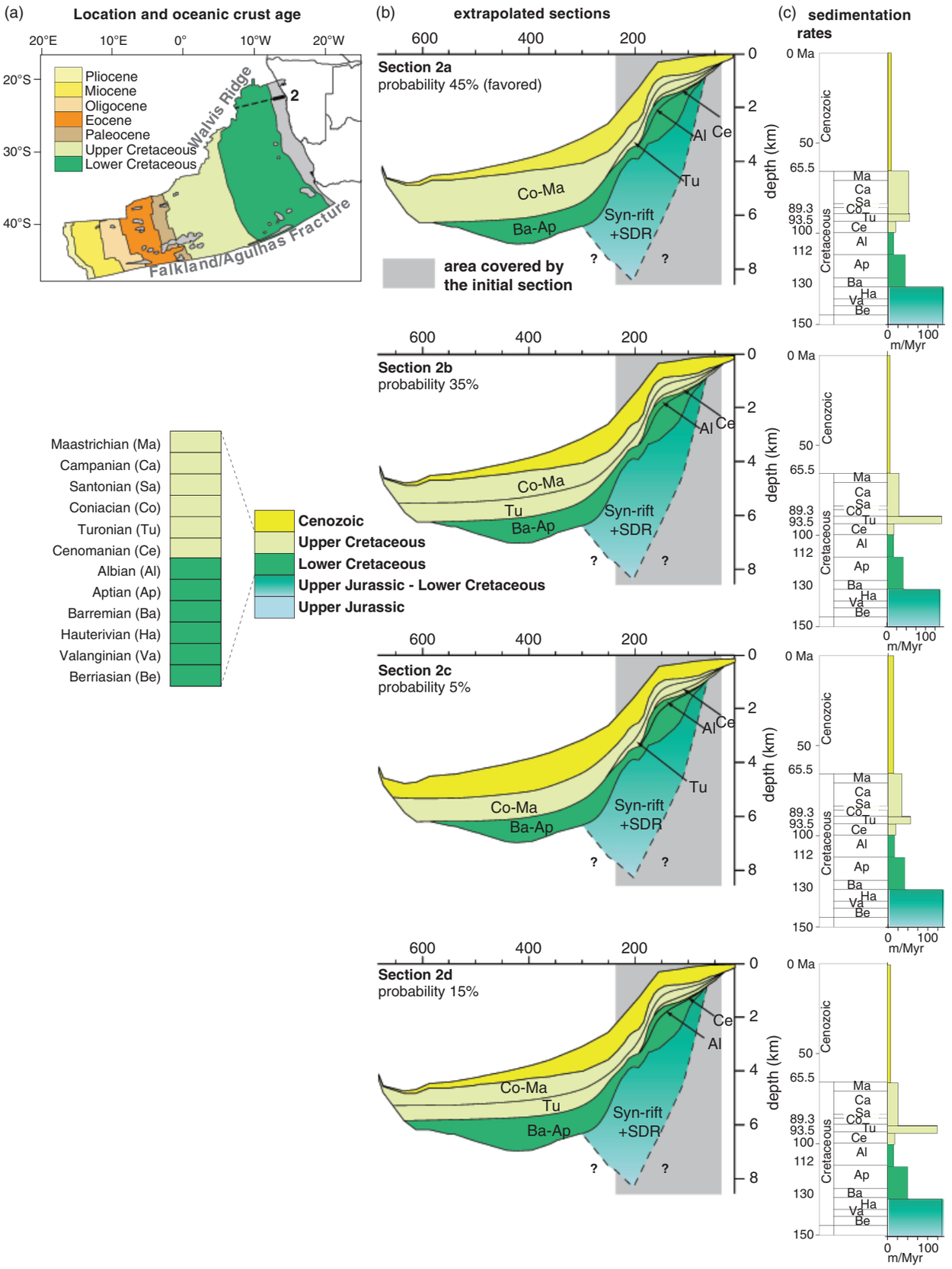

Fig. 7. Detailed results for section 2. (a) Location of the initial (thick black line) and extrapolated (dashed lines) sections and age of the oceanic floor (after UNESCO *et al.*, 1990). (b) Four extrapolation hypotheses are established for section 2 and probabilities associated. The area covered by the initial section is shaded on each section. (c) Rates of accumulation for each section and time increment (mean deposited thickness h_i vs. time). See Table 3 for values. SDR, seaward dipping reflectors.

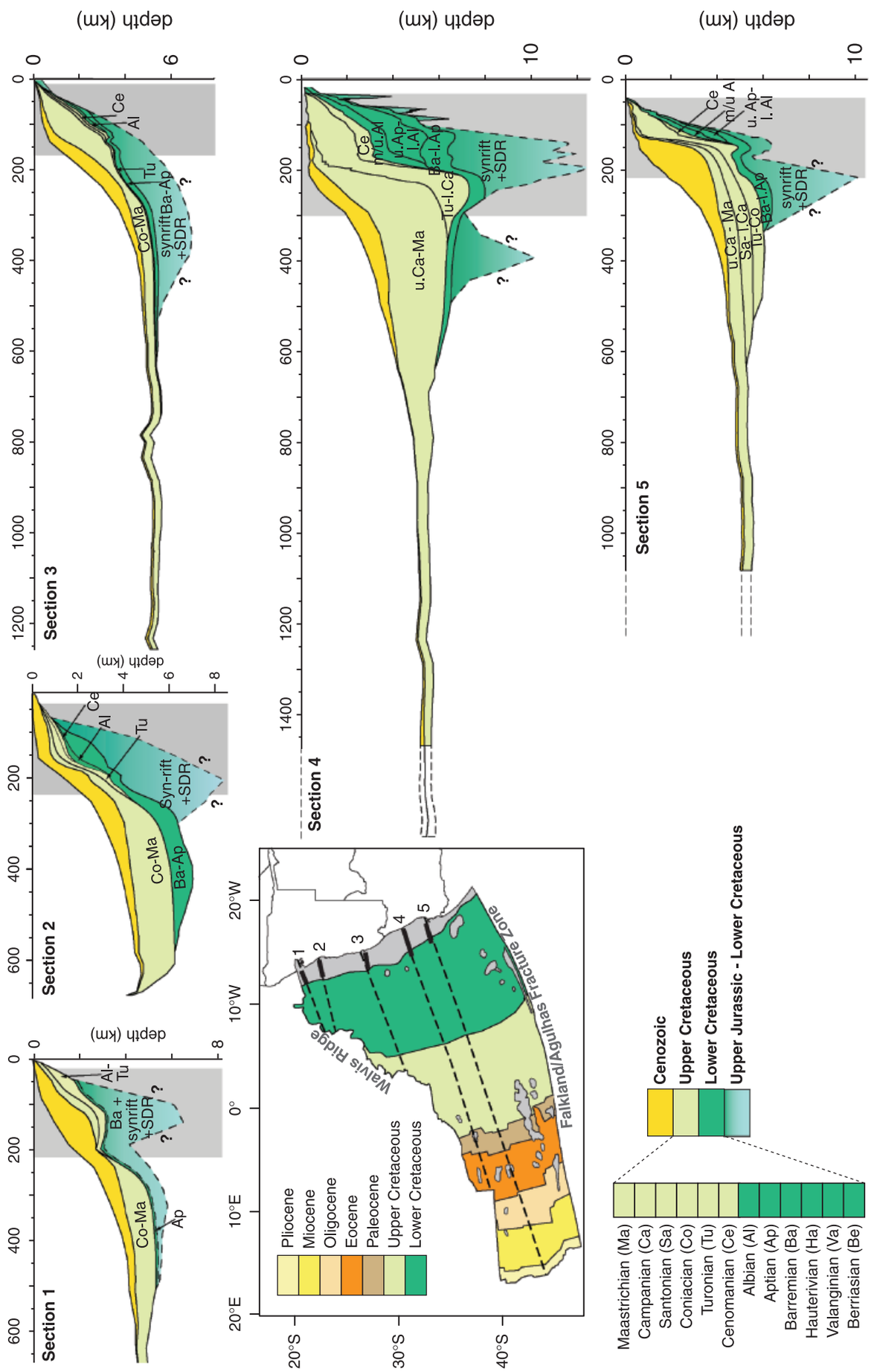

Fig. 8. Extrapolated cross-sections established for the Orange Basin (dashed lines) from the initial published sections (thick black lines) and their location. The age of the oceanic floor is after UNESCO *et al.* (1990). The area covered by the initial sections is shaded on each section. Only the favoured hypothesis for each section is shown. SDR, seaward dipping reflectors.

Corrections for non-terrigeneous contribution

Correction for volcano-clastics and volcanics

In the Orange and Walvis Basins, only the syn-rift geometries include significant amounts of volcanics and volcanoclastics (e.g. Gerrard & Smith, 1982; Light *et al.*, 1993; Van der Spuy, 2003; Hirsch *et al.*, 2010). As the volume of this volcanic contribution is unknown, we were not able to correct them.

Table 3. 2D accumulation rates (mean deposited thickness hi vs. time in m Myr^{-1}) for the extrapolation hypotheses (a–d) of section 2 (see Fig. 7)

Section 2					
		Extrapolation hypothesis			
Time interval	Myr	2a	2b	2c	2d
Cenozoic	0–65.5	6	6	12	6
Coniacian-Maastrichian	65.5–89.3	41	25	28	21
Turonian	89.3–93.5	43	113	45	99
Cenomanian	93.5–99.6	15	14	15	14
Albian	99.6–112	11	13	13	12
Barremian-Aptian	112–130	35	34	34	40
Syn-rift+SDRs	130–150.8	109	109	109	109

SDR, seaward dipping reflectors.

Correction for carbonates

The post-rift sedimentary sequence of the Namibia–South Africa margin is predominantly siliciclastics from an open marine environment ranging from shelf to deep-sea plain (e.g. Dingle *et al.*, 1983; Brown *et al.*, 1995). Nevertheless, evidence of carbonates has been documented for the Middle Cretaceous and Cenozoic on the shelf (e.g. Brown *et al.*, 1995; Bray *et al.*, 1998; Holtar & Forsberg, 2000; Hirsch *et al.*, 2010), along the shallow Walvis Ridge (ODP leg 40 sites 362 and 363; Bolli *et al.*, 1978), as well as in the distal deposits located offshore the Cape peninsula (in hemipelagites: Bolli *et al.*, 1978; Melguen, 1978; DSDP leg 40 sites 360 and 361). We compiled $CaCO_3$ content for available wells (Fig. 13) and estimated a mean carbonate content for each time interval, using end-member values (the minimum and maximum content encountered in the wells for each time interval; see values in Fig. 13). The estimated $CaCO_3$ content ranges between 20% and 40% for the Albian wedge and between 20% and 70% for the whole of the Cenozoic (Fig. 13).

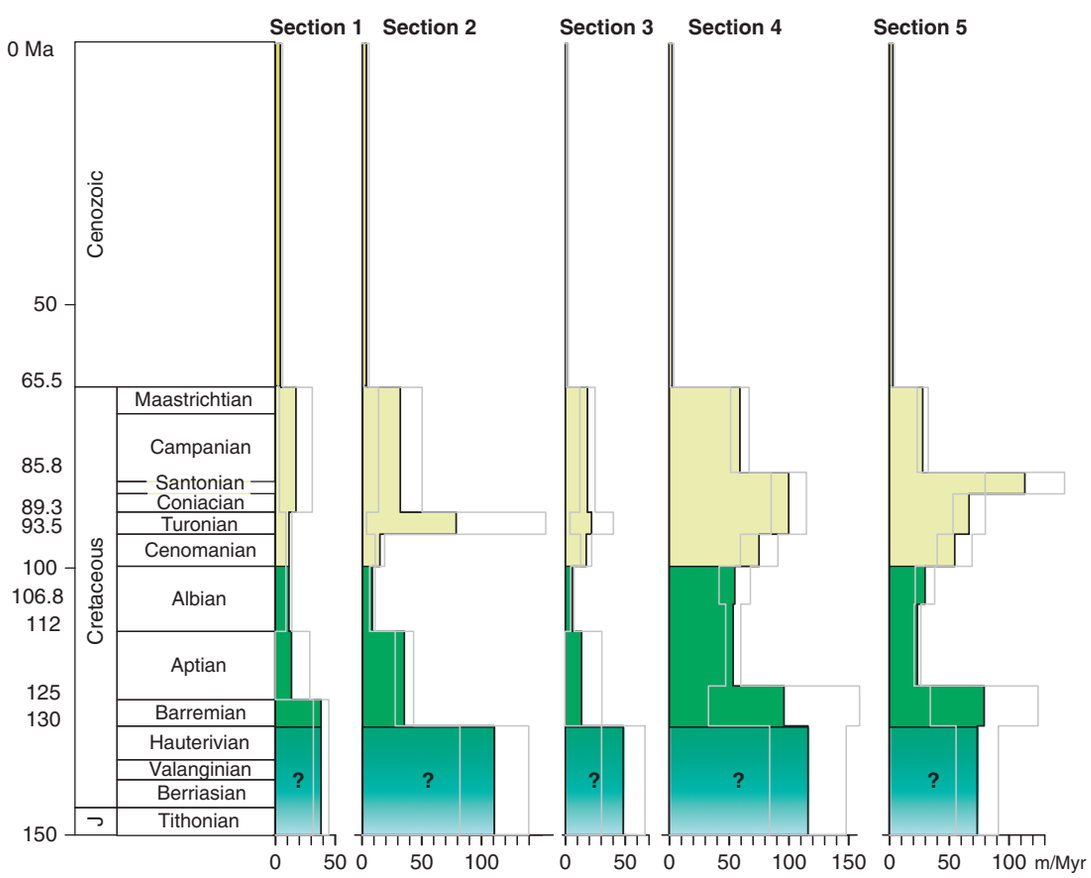

Fig. 9. Rate of sediment accumulation (mean deposited thickness h_i vs. time) determined for sections 1–5 and associated uncertainties. Note that the boundaries of the time increments vary from one section to another. See Table 4 for values.

Table 4. 2D accumulation rates (mean deposited thickness h_i vs. time) and associated variance for sections 1–5 (see Fig. 9)

Time interval	(Myr)	Rate (m Myr^{-1})	σ (m Myr^{-1})
Section 1			
Cenozoic	0–65.5	4	± 2
Coniacian-Maastrichtian	65.5–89.3	17	± 14
Albian-Turonian	89.3–112	11	± 2
Aptian	112–125	13	± 15
Syn-rift+SDRs-Barremian	125–150.8	38	± 6
Section 2			
Cenozoic	0–65.5	4	± 2
Coniacian-Maastrichtian	65.5–89.3	32	± 18
Turonian	89.3–93.5	78	± 75
Cenomanian	93.5–99.6	15	± 4
Albian	99.6–112	9	± 2
Barremian-Aptian	112–130	35	± 8
Syn-rift+SDRs	130–150.8	110	± 29
Section 3			
Cenozoic	0–65.5	2	± 1
Coniacian-Maastrichtian	65.5–89.3	18	± 6
Turonian	89.3–93.5	22	± 18
Cenomanian	93.5–99.6	17	± 5
Albian	99.6–112	6	± 1
Barremian-Aptian	112–130	14	± 17
Syn-rift+SDRs	130–150.8	48	± 18
Section 4			
Cenozoic	0–65.5	2	± 1
Upper Campanian-Maastrichtian	65.5–81.7	59	± 8
Turonian-Lower Campanian	81.7–93.5	100	± 15
Cenomanian	93.5–99.6	75	± 16
Middle Upper Albian	99.6–106.8	55	± 13
Upper Aptian-Lower Albian	106.8–122.4	54	± 6
Barremian-Lower Aptian	122.4–130	96	± 63
Syn-rift+SDRs	130–150.8	116	± 32
Section 5			
Cenozoic	0–65.5	3	± 1
Upper Campanian-Maastrichtian	65.5–81.7	28	± 5
Santonian-Lower Campanian	81.7–85.8	114	± 33
Turonian-Coniacian	85.8–93.5	67	± 14
Cenomanian	93.5–99.6	55	± 15
Middle Upper Albian	99.6–106.8	30	± 8
Upper Aptian-Lower Albian	106.8–122.4	23	± 3
Barremian-Lower Aptian	122.4–130	79	± 45
Syn-rift+SDRs	130–150.8	74	± 18

SDR, seaward dipping reflectors.

Corrections for the remaining porosity

In the case of the Orange–Walvis basin, no porosity data were available in the literature. The procedure to estimate the remaining porosity, is based on the standard exponential porosity–depth law (see Allen & Allen, 1990 for a review of these laws), detailed in Appendix 1. With this procedure, we estimated the remaining porosities for each time increment for each section and used them to reach solid accumulated volumes and rates.

Because, in practice, detailed lithologies are too variable to be adequately described at the basin scale (when they are known at all, it is usually not beyond the platform), we assumed a constant sand/shale ratio within each time interval. We then tested a wide range of sand/shale ratio values (ranging from pure sand to pure clay) and estimated the influence of this sand/shale ratio in the estimation of the accumulated volumes.

Correction for post-depositional sediment redistribution

Post-depositional redistribution of sediments by erosion or deformation will not alter the total volume of sediment measured because sediment eroded for a given time interval will be included in a later time interval. It might

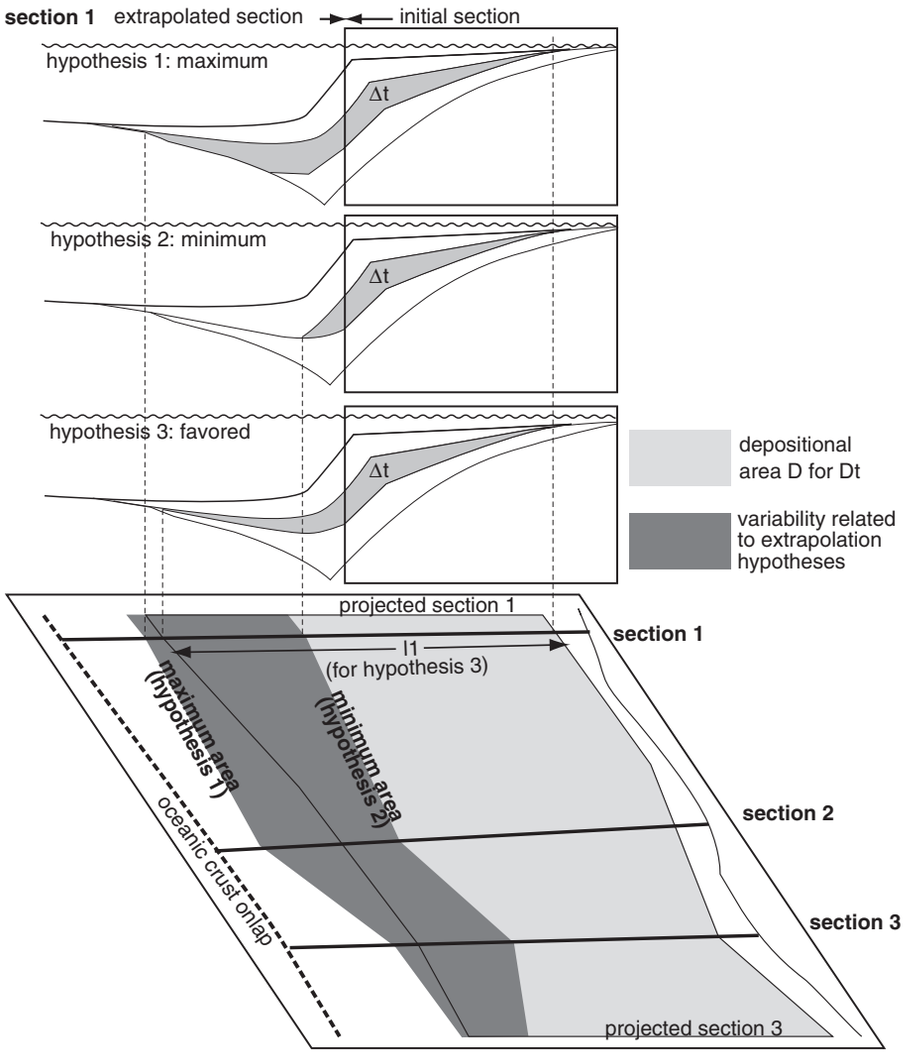

Fig. 10. Principle of mapping the deposition area for each time interval Δt (light grey area). The extent of the deposited wedge is mapped along each section (only section 1 is detailed here) and interpolated from one section to another. The variability associated with the extrapolation step (dark grey area) is estimated from the difference between the different extrapolation hypotheses established for each section.

however modify the incremental volumes (volumes eroded for a given time interval are included in a later one). Our method potentially allows for a correction from this post-depositional erosion (for example, see hypothesis 3 in Fig. 5) by reconstructing the geometry of the deposited wedge before its subsequent erosion for each time interval. On the other hand, the effects of sediment redistribution by deformation such as listric faults are neglected because they are below the resolution of the method (kilometric listric fault induce redistribution at the kilometric scale).

In the case of the Namibia–South Africa margin, two major unconformities associated with erosion have been documented on the platform (e.g. Brown *et al.*, 1995; Clemson *et al.*, 1997; Aizawa *et al.*, 2000; Stevenson & McMillan, 2004; Paton *et al.*, 2007, 2008): a major one (associated with a tilting of the margin) at the end of the Cretaceous and another during the Cenozoic. The Cenozoic event will not alter our results since erosion and re-sedimentation occurred within a single time increment; we will therefore only discuss the late Cretaceous erosion event. The age of the sediments affected by this late Cretaceous erosion varies along the margin from the whole post-rift sequence (e.g. Brown *et al.*, 1995; Stevenson & McMillan, 2004; section 4 in Fig. 4) to only the Upper Cretaceous sequence (e.g. Brown *et al.*, 1995; Clemson *et al.*, 1997; Aizawa *et al.*, 2000; Paton *et al.*, 2007, 2008; sections 3 and 5 in Fig. 4). The age of the unconformity is documented on the Kudu well as uppermost Cretaceous (68–67 Myr) to lowermost Palaeocene (57–53 Myr; McMillan, 1990). Paton *et al.* (2007, 2008) and Hirsch *et al.* (2010) estimated the associated erosion on the platform in the southern part of the Orange Basin at about 300 m. As a consequence, preserved volumes slightly underestimate the Cretaceous denudation (which has been affected by erosion) and slightly overestimate the Cenozoic one (which has have been affected by resedimentation).

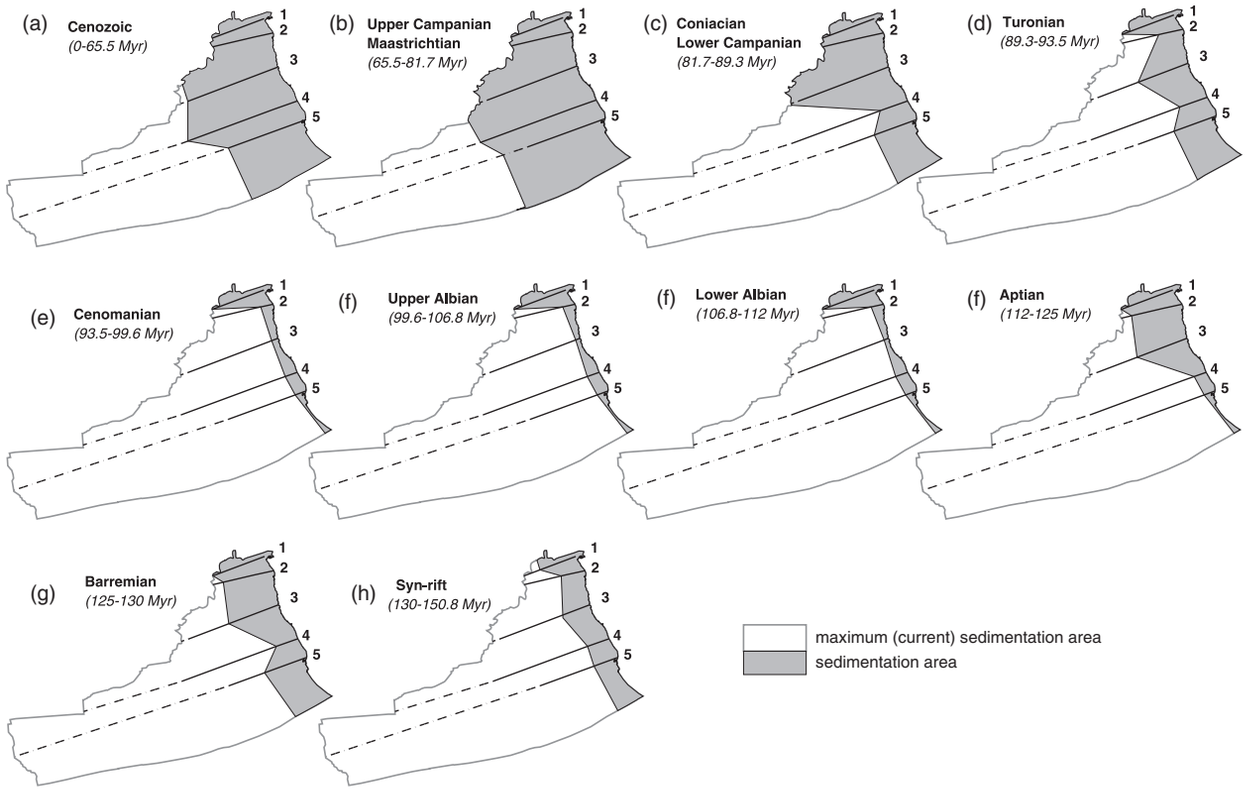

Fig. 11. Deposition area for the 10 time increments used to calculate the deposited volumes. The present day extent of the basin is shown as a grey line and the location of the extrapolated section as black lines. See Table 5 for values.

Table 5. Deposition areas and associated variance of the 10 time increments (see Fig. 11)

Time interval	(Myr)	Deposition area ($\times 10^{12}$ m^2)	σ
Cenozoic	0–65.5	1.859	$\pm$ 0.033
Upper Campanian-Maastrichian	65.5–81.7	1.836	$\pm$ 0.006
Coniacian-Lower Campanian	81.7–89.3	1.200	$\pm$ 0.023
Turonian	89.3–93.5	0.710	$\pm$ 0.268
Cenomanian	93.5–99.6	0.244	$\pm$ 0.083
Upper Albian	99.6–106.8	0.230	$\pm$ 0.053
Lower Albian	106.8–112	0.215	$\pm$ 0.052
Aptian	112–125	0.555	$\pm$ 0.072
Barremian	125–130	0.780	$\pm$ 0.140
Syn-rift+SDRs	130–150.8	0.533	$\pm$ 0.119

SDR, seaward dipping reflectors.

Assuming a maximum configuration scenario in which the late Cretaceous event resulted in a 300 m erosion throughout the platform, which was about 100 km wide at the time, this corresponds to a section area of about 30 km^2. For a basin about 1000 km wide, this corresponds to a mean eroded thickness of 30 m. For an area of the basin about 1.8×10^{12} m^2 in the Uppermost Cretaceous (Table 5; Fig. 11), this results in an eroded volume of about 5.4×10^{13} m^3, i.e. a maximum of 15% of the Cenozoic volume and $<2\%$ of the post-rift Cretaceous volume. Because the age of the sediment affected by this erosion varies a lot spatially and because the total eroded amount is rather limited and restricted to the platform, we chose to not reconstruct the geometry of the deposited wedge before its subsequent erosion for every time interval. Instead, we included the corrections estimated above into our uncertainty estimation.

Correction for long-shore transport

Long-shore sediment transport related to oceanic circulation may either increase or reduce the volume of sediment

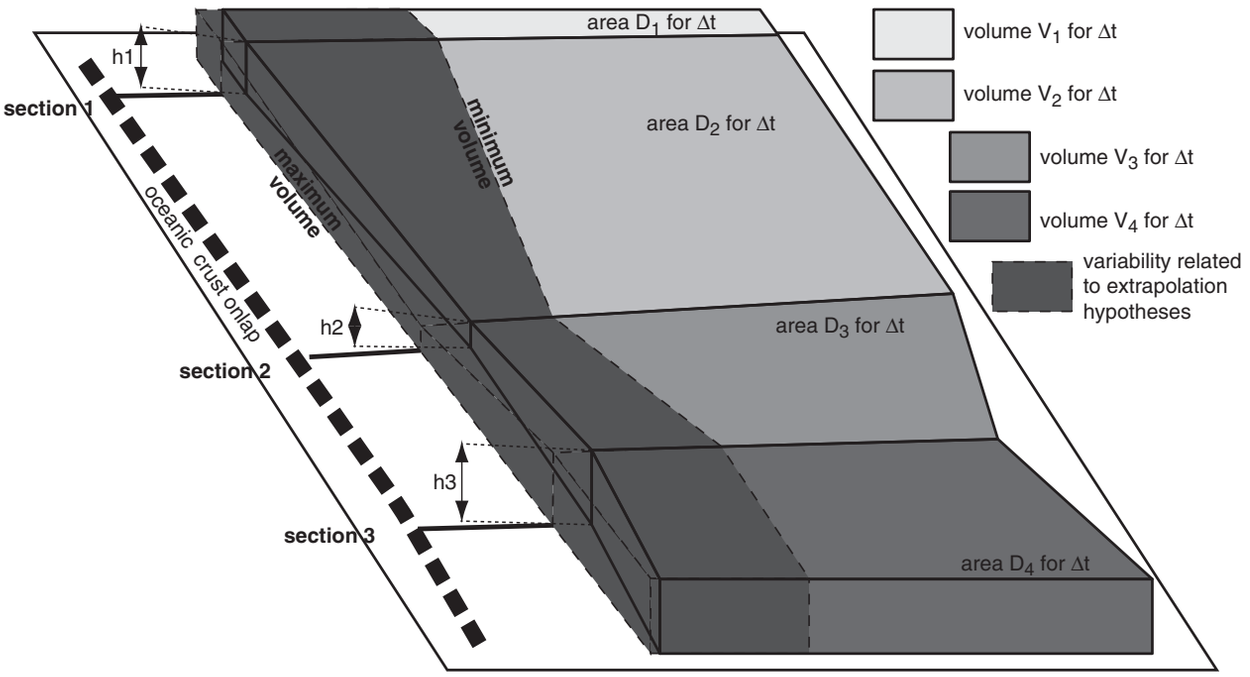

Fig. 12. Volume of sediment deposited for time interval Δt. The deposition area is subdivided into elementary polygons bounded by the cross-sections. The volume of deposited sediments for each polygon (V_i) is determined from its area (D_i) and the interpolated deposition thickness between cross-sections $\frac{h_i+h_{i+1}}{2}$. The total volume of sediment deposited for the time interval is the sum of these elementary volumes $V = \Sigma V_i$.

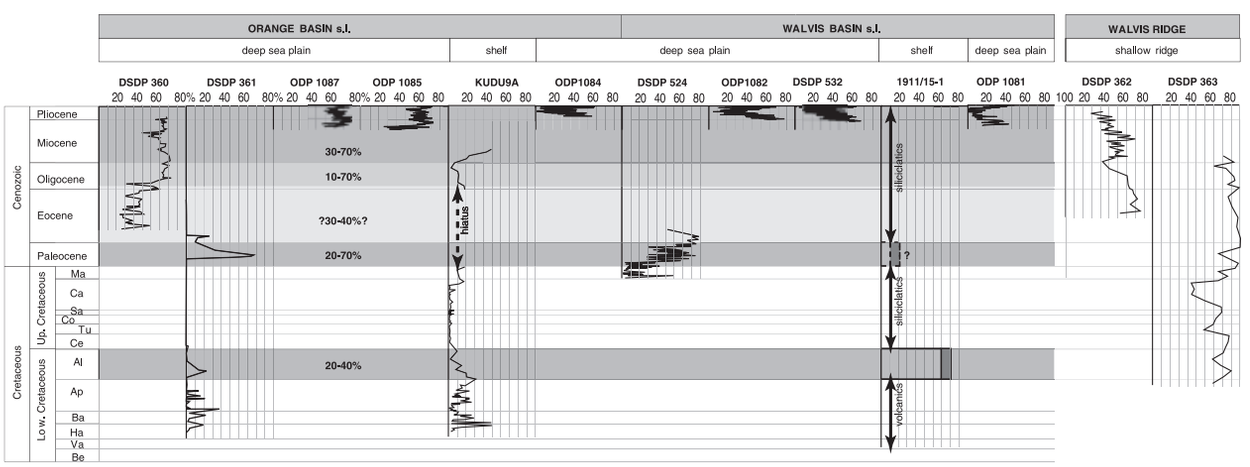

Fig. 13. $CaCO_3$ content for wells available in the literature (see location in Fig. 3). After DSDP/ODP reports (Wefer *et al.*, 1998; Bolli *et al.*, 1978; Moore *et al.*, 1984) for legs DSDP 40 (360, 361, 362, 363), DSDP 74 (524, 532) and 178 (1081, 1082, 1084, 1085, 1087), Wickens & McLachlan (1990) and McMillan (1990, 2003) for Kudu9A well, Bray *et al.* (1998) for well 2112/13-1 and Holtar & Forsberg (2000) for well 1911/15-1. Bold figures indicate the $CaCO_3$ content estimates for the considered time intervals (grey intervals).

accumulated in the study area. To address this, we defined a study area large enough to include long-shore sediment transport from the Walvis Ridge to the Aghulas Fracture Zone (Fig. 3). However, this does not account for northward sediment transport over the Walvis Ridge associated with the Benguela current (e.g. Siesser, 1980; Tucholke & Embley, 1984; Berger *et al.*, 2002; Uenzelmann-Neben *et al.*, 2007) or over the Aghulas fracture zone (Uenzelmann-Neben *et al.*, 2007). The volumes of sediments transported by these currents are unknown; however, they initiated during the Cenozoic (e.g. Siesser, 1980; Tucholke & Embley, 1984; Berger *et al.*, 2002; Uenzelmann-Neben *et al.*, 2007) and will only affect the evaluation for this period.

Accumulated volumes and rates along the Namibia–South Africa margin

Since the boundaries of the time intervals vary from one section to another, we homogenized the temporal resolution of the measurements by recalculating the deposited thickness and sedimentation rates for the shortest common time interval. We obtained a final temporal resolution of one time increment for the Cenozoic, four for the Upper

Cretaceous and five for the Lower Cretaceous (Tables 6 and 7). Figure 14 shows the volume of terrigeneous solid sediment accumulated in the basin and accumulation rates. We also estimated the associated variance related to (i) the extrapolation step, (ii) the spatial variability of seismic velocities for the depth conversion, (iii) the uncertainty on the absolute ages of stratigraphic horizons (see Table 6), (iv) the uncertainties in the estimation of the carbonate content and (v) the sand/shale ratio for the remaining porosity estimation. These uncertainties and their evaluation procedure are detailed below ('Resolution and source of uncertainties').

The volumes of sediments preserved in the basin decreased (from about 10×10^{14} to $0.2 \times 10^{14}\,m^3$) between the syn-rift and the lower Albian (between 150.8 and 106.8 Ma), then increased to reach a major peak (of about $11.5 \times 10^{14}\,m^3$) in the Campano-Maastrichian (between 81.7 and 65.5 Ma) and finally decreased again (to about $3.5 \times 10^{14}\,m^3$) in the Cenozoic (65.5–0 Myr). In terms of accumulation rates, the behaviour is similar: they decreased from about $4.8 \times 10^{13}\,m^3\,Myr^{-1}$ at 150.8 Ma to $0.4 \times 10^{13}\,m^3\,Myr^{-1}$ at 106.8 Ma, and then increased to a maximum rate of about $7.2 \times 10^{13}\,m^3\,Myr^{-1}$ at 89.3 followed by a decrease below $0.5 \times 10^{13}\,m^3\,Myr^{-1}$ during the Cenozoic.

Table 6. Age of the stratigraphic horizons and associated uncertainties used for the accumulation rates and volumes calculation (after ICS, 2004)

Time line = boundary	Age (Myr)	Uncertainty (Myr)
Maastrichtian/Cenozoic	65.5	± 0.3
Lower/Upper Campanian	81.7	± 0.7
Coniacian/Santonian	85.8	± 0.7
Turonian-Conacian	89.3	± 1
Cenomanian-Turonian	93.5	± 0.8
Albian-Cenomanian	99.6	± 0.9
Lower/Upper Albian	106.8	± 1
Aptian/Lower Albian	112	± 1
Lower/Midle Aptian	124.4	± 1
Barremian/Aptian	125	± 1
Hauterivian/Barremian	130	± 2
Syn-rift+SDRs	150.8	± 4

SDR, seaward dipping reflectors.

RESOLUTION AND SOURCE OF UNCERTAINTIES

To assess the uncertainties related to the various steps of our method, we used a statistical approach. We generated normal distributions of 100 000 samples combining the variability of each parameter (seismic velocity, shale to sand ratio, carbonate content and age of stratigraphic horizons). For the extrapolation step, each hypothesis was given a weight (probability), which was used to select one interpretation per line for each sample of the distribution. These distributions were in turn used to compute probability density functions (PDF) of the sedimentary volumes and sedimentation rates. These PDFs for each time interval are shown in Fig. 15. Although some of them deviate from a Poisson's distribution, we used them to compute a mean and standard deviation for the sedimentary volumes and sedimentation rates. These standard deviations were in turn used to compute 95% confidence intervals used to produce the error estimates shown in Fig. 14.

Uncertainties in the extrapolation step

To assess the influence of the extrapolation step, we systematically tested several extrapolation hypotheses (see 'Principle') to evaluate uncertainties related to the geometry of the sedimentary wedge in the distal part of the basin (see the example of section 2 in Fig. 7). In the case study, the associated variance ranges from 8% to 43% of the accumulated volumes of sediments and rates.

Uncertainties in seismic velocities

We depth converted the three sections that were available only in two-way travel time (sections 1–3; after Aizawa *et al.*, 2000). We assumed a homogeneous velocity within three time-intervals (i.e. syn-rift, Cretaceous and Cenozoic, Fig. 4) and for sections 2 and 3, we also used different

Table 7. Accumulated solid volumes, rates and associated variance (see Fig. 14)

Time interval	(Myr)	Volume ($10^{14}\,m^3$)	σ	Rate ($10^{13}\,m^3\,Myr^{-1}$)	σ
Cenozoic	0–65.5	3.531	± 1.657	0.539	± 0.253
Upper Campanian-Maastrichian	65.5–81.7	11.523	± 1.570	7.113	± 0.969
Coniacian-Lower Campanian	81.7–89.3	5.534	± 0.823	7.281	± 1.082
Turonian	89.3–93.5	2.206	± 0.897	5.253	± 2.137
Cenomanian	93.5–99.6	0.520	± 0.150	0.853	± 0.246
Upper Albian	99.6–106.8	0.421	± 0.094	0.584	± 0.130
Lower Albian	106.8–112	0.249	± 0.049	0.479	± 0.095
Aptian	112–125	3.179	± 0.902	2.446	± 0.694
Barremian	125–130	2.361	± 1.111	4.721	± 2.222
Syn-rift+SDRs	130–150.8	10.064	± 2.535	4.839	± 1.219

SDR, seaward dipping reflectors; Up., upper, Low., lower.

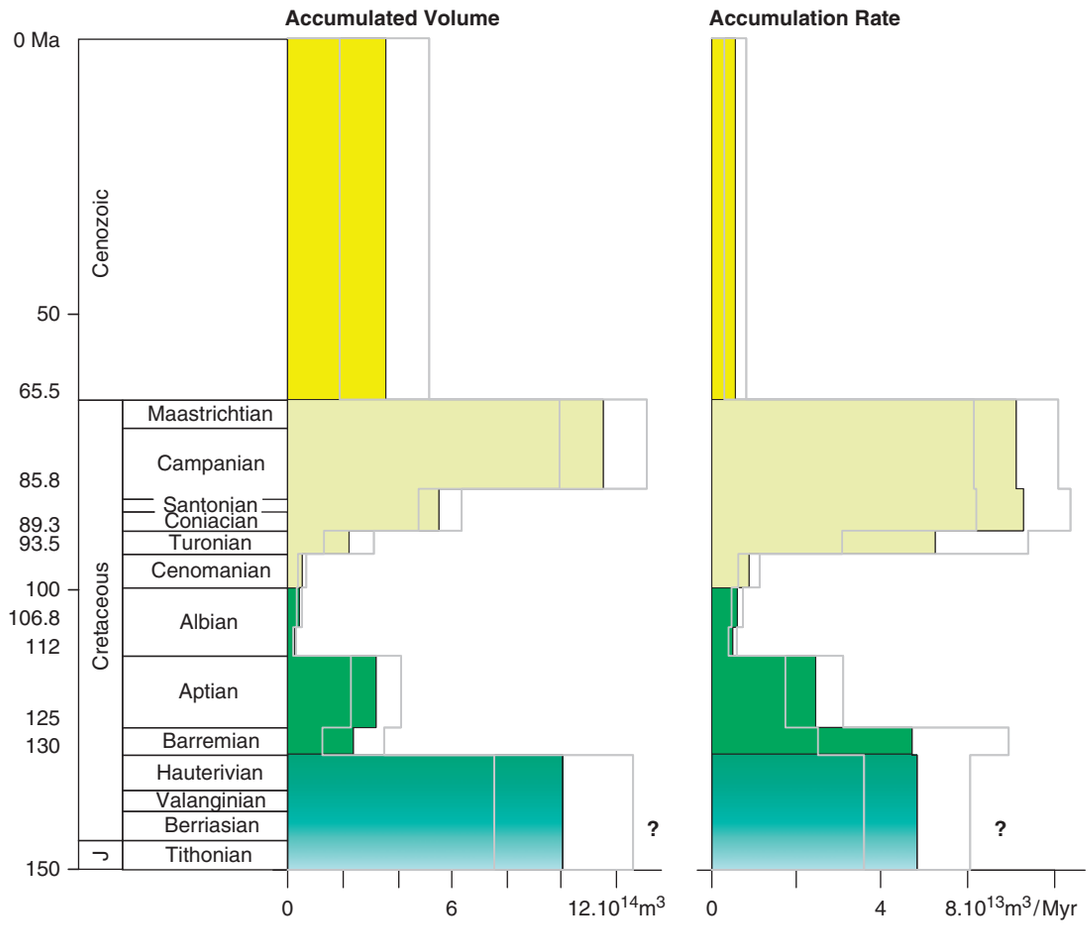

Fig. 14. Accumulated volumes and rates. The temporal resolution of the measurements has been homogenized by recalculating the volumes and sedimentation rates for the shortest time interval encountered among the sections: one time step for the Cenozoic, four for the Upper Cretaceous and five for the Lower Cretaceous. Variance corresponding to the variability between the extrapolation hypotheses, uncertainties on horizon age, carbonate content, sand/shale ratio and seismic velocities are shown.

values for the shelf and distal domains (Table 2). We then estimated the spatial variability of the interval seismic velocities: about $\pm$ 10% (from $\pm$ 7% in the Cenozoic to $\pm$ 13% in the Lower Cretaceous) according to Emery *et al.* (1975). The associated variance ranges from 2% to 10% of the accumulated volumes of sediments and rates.

Uncertainties in the stratigraphic horizon absolute ages

We used the uncertainties on absolute ages of stratigraphic horizons given by ICS (2004; see Table 6). In the case study, the associated variance ranges from 0.2% to 12% of the accumulated volumes of sediments and rates.

Uncertainties in the correction for carbonates

We estimated $CaCO_3$ content ranges between 20% and 40% for the Albian wedge and between 20% and 70% for the whole of the Cenozoic (Fig. 13). The associated variance ranges from 0.2% to 12% of the Albian and is 46% of the Cenozoic.

Uncertainties in the corrections for the remaining porosity

We assumed a constant sand/shale ratio within each time interval and tested the distribution of sand/shale ratios between pure clay and pure sand end members. The associated variance ranges from 3% to 5% of the accumulated volumes of sediments and rates.

DISCUSSION

Validation of the method: comparison with previous results

Rust & Summerfield (1990) and Rouby *et al.* (2009) previously estimated the solid volumes of sediments accumulated along the Namibian-South African margin using isopach maps available in the literature (e.g. Emery *et al.*, 1975; Dingle *et al.*, 1983). Their approach allows volumes to be estimated without an extrapolation step, assuming that these published isopach maps (Emery *et al.*, 1975; Dingle *et al.*, 1983) are accurate. However, these basin scale maps

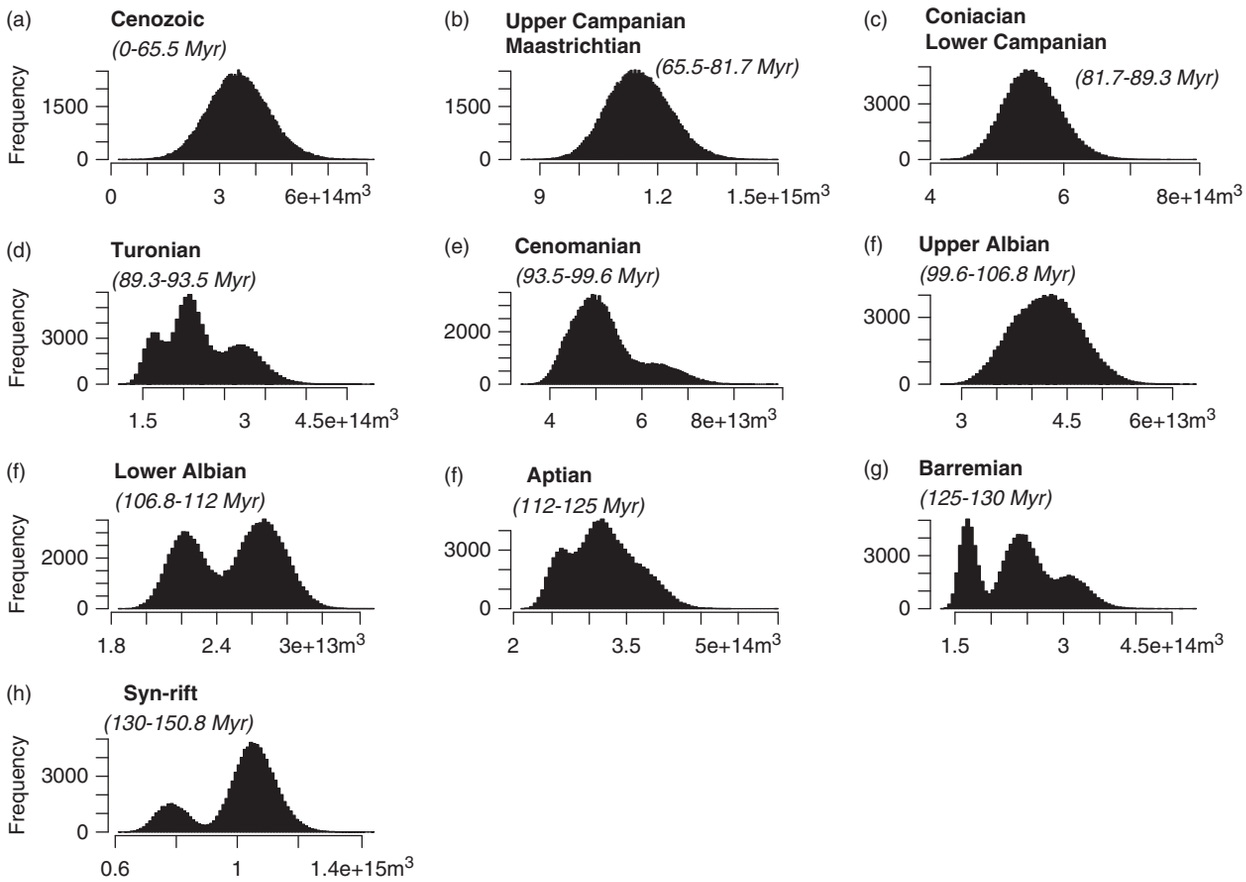

Fig. 15. Probability density functions of the sedimentary volumes for each time interval from the syn-rift (h) to the cenozoic (a).

were available for only four intervals over the studied 130 Myr period. The resulting determination of volumes was therefore at a much lower temporal resolution than our 2D approach for the Cretaceous interval. Also, we used independent source of seismic data (i.e. Brown *et al.*, 1995; Aizawa *et al.*, 2000; Fig. 4) and compiled numerous other sources either seismic (e.g. Emery *et al.*, 1975), biostratigraphic (e.g. McMillan, 1990, 2003; Stevenson & McMillan, 2004) or well-data (e.g. Bolli *et al.*, 1978; Melguen. 1978; Bray *et al.*, 1998; Holtar & Forsberg, 2000). Although, their procedure for correcting *in situ* sedimentation and remaining porosity are similar to ours, Rust & Summerfield (1990) and Rouby *et al.* (2009) did not however perform a detailed uncertainty analysis of their results like ours. Finally, they did not correct the accumulated volumes from carbonate content. These previous works provided us nonetheless with a low temporal resolution reference to discuss the reliability of our method. To compare our results, we recalculated them for similar time increments (i.e. Lower and Upper Cretaceous and Cenozoic time steps; Fig. 16).

Because the data sets are different in each estimations [correlation of 2D cross-section in this study; isopach maps from Dingle *et al.* (1983) in Fig. 16b; isopach maps from Emery *et al.* (1975) in Fig. 16c; a combination of both in Fig. 16d], we do not expect a perfect fit. Furthermore, the volumes deduced by Rouby *et al.* (2009) from data provided by Emery *et al.* (1975) are associated with large uncertainties due to the depth conversion of the initial isopach maps (Fig. 16c). Despite these limitations, our results at a degraded resolution fall within the same order of magnitude as the ones estimated in these previous works (about 10^{14} m^3). Within the associated uncertainties, the values for the Lower Cretaceous (including the syn-rift deposits) and Cenozoic are compatible. The major difference lies in the Upper Cretaceous volume, which is much larger in our results than in the cases of volumes deduced by Rouby *et al.* (2009) from Dingle *et al.* (1983) or by after and Rust & Summerfield (1990) from Dingle *et al.* (1983) and Emery *et al.* (1975).

Interestingly, our results are also in good agreement with the volumes of sediments preserved along the southern margin of South Africa determined by Tinker *et al.* (2008b). Their approach is based on detailed subsurface data (isopach maps and wells) in the proximal part of the southern Cape Basins, with similar corrections for remaining porosity and temporal resolution (four time increments for the Cretaceous, one for the Cenozoic). These two domains are similar in terms of geodynamic evolution (extensional basins with a domain in erosion located on the southern African plateau and its rims). Volumes determined in the southern Cape basins are within

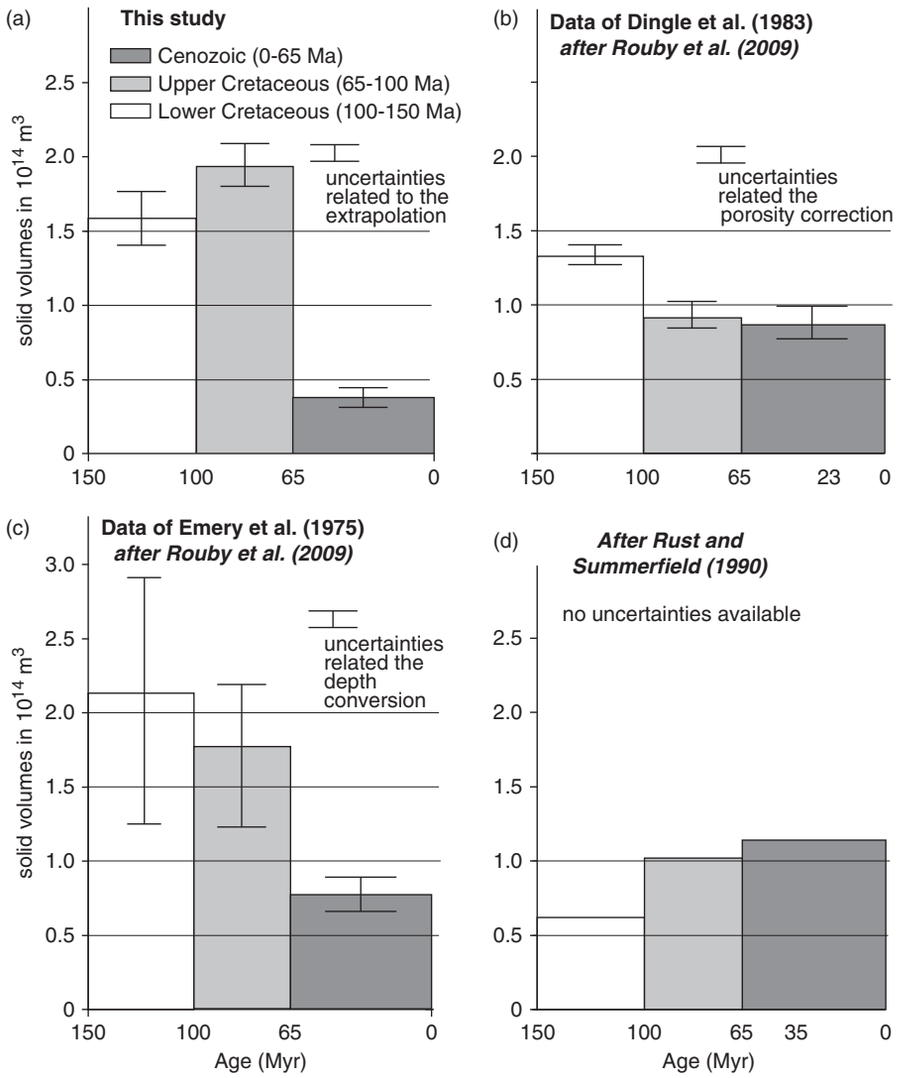

Fig. 16. Comparison of our results with previous works. (a) Solid volumes determined in this study at low temporal resolution. Variance corresponding to the variability between the extrapolation hypotheses, uncertainties on horizon age, carbonate content, sand/shale ratio and seismic velocities are shown. (b) Solid volumes determined by Rouby *et al.* (2009) after data from Dingle *et al.* (1983). Uncertainties due to porosity removal are shown by error bars. (c) Solid volumes determined by Rouby *et al.* (2009) after data from Emery *et al.* (1975). Uncertainties due to depth conversion are shown by error bars. (d) Solid volumes determined by Rust & Summerfield (1990).

the same magnitude range (between 0.3×10^{14} and $0.9 \times 10^{14}\,m^3$) as the one determined in our study (between 0.2×10^{14} and $11.5 \times 10^{14}\,m^3$), although they are slightly lower. This is to be expected since the southern Cape basins are slightly smaller than the Walvis-Orange Basin and the volumes determined there only include proximal parts of the margin. The trends in volumes of sediment accumulated and rate determined for both margins are alsovery consistent: a decrease in the lower Cretaceous, a peak (about $10^{14}\,m^3$) in the Upper Cretaceous and a decrease in the Cenozoic.

Our estimates of the accumulated volume are thus in good agreement with previous studies for the same area either at a lower temporal resolution (Rust & Summerfield, 1990; Rouby *et al.*, 2009) or at similar resolution for an adjacent basin along the southern margin of Africa (Tinker *et al.*, 2008b). The timing of the erosion event at the end of the Cretaceous is also consistent with cooling histories established either in the drainage areas of the margin (Gallagher & Brown, 1999a, b; see location on Fig. 3) or along the southern African margin (Tinker *et al.*, 2008a) that both determined a large denudation event at the end of the Cretaceous to model the cooling ages.

Some insights into the possible causes of the evolution of the siliclastic budget of the Namibian and South African margins

Beyond the validation of our approach on a well-constrained case study, our results provide an estimation of solid terrigeneous sediment accumulation at the basin scale at a better resolution for the Cretaceous interval than previously published data sets for the Namibia–South

Africa margin. They show that sediment accumulation rates vary significantly through time, both in terms of volumes and sedimentation rates (Fig. 14). These can be described in four periods: two of high siliciclastic accumulation during the (1) Hauterivian-Aptian (136–112 Myr) and (3) Turonian-Maastrichian (93–65 Myr) alternating with two lows during the (2) Albian-Cenomanian (112–93 Myr) and (4) Cenozoic (65–0 Ma). Variations in sediment accumulation rates are related to either relief variations in the drainage area or reorganization of the drainage system (capture). In this case, the latter has never been documented, therefore accumulation are more probably related to relief variations that are triggered either by deformation (rock uplift variations in the drainage areas) or climate (long term precipitation change altering erosivity in the drainage area; e.g. Bonnet & Crave, 2003). Below, we provide a brief analysis of the possible causes of relief variation along the Namibia–South Africa margin.

(1) During the syn-rift (150–130 Myr), significant volumes of sediments were preserved (over $10 \times 10^{14}\,m^3$ and $5 \times 10^{13}\,m^3\,Myr^{-1}$). The supply then decreased during the Aptian (about $4 \times 10^{14}\,m^3$ and $3 \times 10^{13}\,m^3\,Myr^{-1}$). Since the drift onset took place at the end of the Hauterivian, the relief variations causing this important sedimentary supply can safely be attributed to the erosion of some rift-related relief (without constraints on whether or not they have actually been expressed in the topography). Furthermore, the decrease in terrigeneous sediment supply toward the basin during the subsequent 10–20 Myr is the expected behaviour for the relaxation of this rift-related relief.

(2) The Lower Albian corresponds to the absolute minimum of sediment accumulation since 150 Myr (lower than $0.25 \times 10^{14}\,m^3$ and $0.6 \times 10^{13}\,m^3\,Myr^{-1}$) and marks the end of the decrease in the sediment accumulation described above. This is consistent with the development of a carbonate platform in the Walvis Basin (Fig. 13; e.g. Holtar & Forsberg, 2000). It is also coeval with significant retrogradation of the shelf (Brown *et al.*, 1995; Paton *et al.*, 2008; see the Albian wedge on the shelf in Fig. 8). This retrogradation is consistent with a very low sedimentary supply, lower than the thermal and flexural subsidence of the post-rift margin 30 Myr after the drift onset (break-up unconformity), resulting in the retrogradation of the shelf. The horizontal amplitude of this retrogradation is also consistent with the absence of important reliefs near the coastline at the time. Also, no significant climate change has been documented in the Lower Albian in southern Africa (e.g. Chumakov *et al.*, 1995). These observations suggest that the low sedimentation rates of the Albian can be attributed to the complete erosion of the rift-related relief (or scarp retreat) starving the basin. The accumulation then slightly increased twofold during the Upper Albian and Cenomanian (*ca*. $0.5 \times 10^{14}\,m^3$ and $0.8 \times 10^{13}\,m^3\,Myr^{-1}$).

(3) The accumulation increased further, at first slowly during the Turonian, Coniacian and Santonian (93.5–85.8 Myr), and then rapidly to form the major peak of the Campano-Maastrichian (about $11 \times 10^{14}\,m^3$, about $7 \times 10^{13}\,m^3\,Myr^{-1}$). This maximum in both accumulated volumes and rates, well exceeding Lower Cretaceous values, implies a significant relief reorganization more than 50 Myr after the rifting event. It is coeval with the tilting and uplift event documented on the platform at the end of the Cretaceous (e.g. Brown *et al.*, 1995; Clemson *et al.*, 1997; Aizawa *et al.*, 2000; Stevenson & McMillan, 2004; Paton *et al.*, 2007, 2008; Hirsch *et al.*, 2010). This major peak in sedimentation rate has also been documented along the southern margin of the South African plateau (Tinker *et al.*, 2008b). It is coeval with important denudations, documented by thermochronology, along both the western and southern margins (Gallagher & Brown, 1999a, b; Brown *et al.*, 2002; Raab *et al.*, 2002, 2005; Tinker *et al.*, 2008a). This relief reorganization therefore affected both margins of the southern African plateau and resulted in an increase of siliciclastic accumulation in the Uppermost Cretaceous (93.5–65.5 Myr) and associated denudation along the western and southern margins.

It could be caused by both a major change in the rock uplift rate in the drainage basins feeding these basins (potentially associated with an uplift of the South African plateau) or an evolution toward wetter conditions at that time. These causes are not mutually exclusive. Several authors have suggested an uplift of the southern African plateau in the late Cretaceous (Gallagher & Brown, 1999a, b; de Wit, 2007; Tinker *et al.*, 2008a, b). However, this is highly debated (e.g. Partridge & Maud, 1987; Burke, 1996; Burke & Gunnell, 2008). From a climatic point of view, Chumakov *et al.* (1995) suggested a change from hot arid conditions in the Cenomanian (100–93 Myr) to warmer and more humid ones in the Santono-Maastrichitian (85–65.5 Myr). This is confirmed by palynologic analyses of Upper Cretaceous kimberlite pipes which indicate slightly warmer and wetter conditions (e.g. Scholtz, 1985; Smith, 1986; Rayner *et al.*, 1991).

(4) For the Cenozoic period, the total deposited volume is about $5 \times 10^{14}\,m^3$ (for a mean deposition rate of roughly $10^{13}\,km^3\,Myr^{-1}$), i.e. much lower than the late Cretaceous and within the same order of magnitude as during the Aptian and Albian (between 125 and 100 Myr). This low siliciclastic accumulation rate is consistent with the development of carbonate sedimentation at the time (Fig. 14; e.g. Dingle *et al.*, 1983; Holtar & Forsberg, 2000). A similar reduced sedimentation rate has also been recorded along the southern margin of the plateau at the same time (Tinker *et al.*, 2008b).

This decrease suggests limited relief reorganization during the Cenozoic, compared with the reorganiza-

tion that occurred in the late Cretaceous. It can be related to a low amount of relief creation (limited rock uplift) or to aridity in the drainage areas limiting the erosivity, and in doing so, limiting relief variations. Again, these two effects are not mutually exclusive. Evidence of uplift is documented on the platform domain margin during the Cenozoic (e.g. Brown *et al.*, 1995; Clemson *et al.*, 1997; Aizawa *et al.*, 2000; Stevenson & McMillan, 2004; Paton *et al.*, 2007, 2008; Hirsch *et al.*, 2010). However, the exact timing is not well constrained: Paton *et al.* (2008) and Hirsch *et al.* (2010) suggested a Burdigalian-Langhian age (16–14 Myr), whereas Mcmillan (1990) documented Burdigalian sediments above the unconformity in the Kudu well. In addition, an aridification has been documented along the Namibia Margin during the Middle Miocene (development of large aeolian deposits; e.g. Pickford *et al.*, 1996; Ségalen *et al.*, 2002, 2004; Senut *et al.*, 2009). However, our data are not detailed enough to further discuss the causes of this accumulation decrease.

CONCLUSIONS

We developed and tested a simple approach to quantify terrigeneous solid volumes accumulated in sedimentary basins and the associated uncertainties, taking into account the whole sedimentary basin from the onshore continental onlap down to the most distal deepest marine deposits (over the oceanic crust in the case of passive margins). The volume of sediments was estimated from the interpolation of a series of cross-sections established from the extrapolation of published cross-sections, usually limited to the most proximal part of the margin. For each time interval of each section, the mean deposited thickness and the area of deposition were measured, and from this, the accumulated volume was calculated. We first measured the total volume of accumulated sediments, then estimated the *in situ* production (e.g. carbonates, volcano-clastics, volcanics) and remaining porosity in order to correct the accumulated volumes.

Using this approach, we quantified the sediment accumulation history volume along the Namibia–South Africa margin based on five cross-sections.

(i) We determined by a statistical approach the variances associated with each parameter of the method: the geometrical extrapolation of the section (8–43%), the uncertainties on seismic velocities for the depth conversion (2–10%), on the absolute ages of stratigraphic horizons (0.2–12%), on the carbonate content (0.2–46%) and on remaining porosities estimation (3–5%). Our estimates of the accumulated volumes were validated by comparison with previous estimates at a lower temporal resolution in the same area.

(ii) From this, we first obtained a description meso-cenozoic sedimentary wedge at the Orange-Walvis Basin showing a first-order evolution that was consistent along the margin (retrograding Lower Cretaceous, prograding Upper Cretaceous and Cenozoic) with significant spatial variability in terms of preserved thicknesses.

(iii) We documented a major increase of the area of deposition during the Upper Cretaceous (10 × about 80 Myr ago) as well as significantly larger 2D sedimentation rates in the southern part of the basin (Orange Basin).

(iv) The solid volumes accumulated along the Namibian–South African margin vary significantly through time, both in terms of volumes and sedimentation rates. They show four periods: two periods of high siliciclastic accumulation during the Hauterivian-Aptian (136–112 Myr) and Turonian-Maastrichian (93–65 Myr), which could be attributed to relief reorganization triggered by climate and/or deformation. They alternate with two periods of low accumulation during the Albian-Cenomanian (112–93 Myr) and Cenozoic (65–0 Ma), which could be related to a period without significant relief or moderate relief reorganization.

From a methodological perspective, to further discuss the balance between denudation on the continent and sedimentation in the adjacent basins, the chemical component of the denudation evaluation should be integrated. Since this contribution is not recorded in the siliclastic supply of basins, the part of the relief dynamics related to chemical erosion is neglected in our approach. One approach to resolve this issue would be to examine the mineralogy and chemistry of terrigeneous minerals in the basin sediments and possibly *in situ* alteration products.

ACKNOWLEDGEMENTS

We thank Dr Sarah Mullin for post-editing the English style. We are thankful to Kevin Burke for a thorough review of an early version of the manuscript as well as to Nick Harris, Mike Blum and Jeffrey Nunn for their very constructive comments. This work had been funded by the CNRS/INSU 'Relief de la Terre' and 'ECLIPSE' programs between 2004 and 2006 as well as the ANR 'TOPOAFRICA' (2009–2013).

APPENDIX 1: REMAINING POROSITY CORRECTION

Terrigeneous volumes and rates are corrected for the remaining porosity. To estimate this, we used the standard exponential porosity-depth law described by Sclater & Christie (1980) for sediments in the North Sea Basin. This assumes porosity (ϕ) is reduced under hydrostatic conditions (with no cementation, overburial or erosion), and porosity is an exponential function of depth, z, i.e.

Table 8. Parameter values for the remaining porosity correction

	Clay	Sand	Water
ϕ_o (%)	0.63	0.49	
c (km^{-1})	0.27	0.51	
ρ ($kg\,m^{-3}$)	2650	2750	1000

$$\phi(z) = \phi_0 e^{-cz}$$

where ϕ_0 and c are lithology-dependent parameters.

The solid grain volume, V_s, is given as

$$V_s = (1 - \bar{\phi})V_T$$

where V_T is the total observed volume and $\bar{\phi}$ is average porosity between depths z_1 and z_2 given as

$$\bar{\phi} = (1/(z_2 - z_1)) \int_{z_1}^{z_2} \phi(z)dz$$

For the exponential porosity-depth dependence, we have

$$\bar{\phi} = (\phi_0/c)(e^{-cz1} - e^{-cz2})/(z_2 - z_1)$$

In the case of the Orange basin, no porosity data are available in the literature. We used the porosity law of Sclater & Christie (1980; Table 8). Although this law has been defined for the North Sea area, its specificity actually resides in the carbonate component (chalk) that we do not use here. Pure lithologies in sand and clay of Sclater & Christie (1980) porosity laws do cover lithologies estimated in the Orange Basin (sand/shale ratio).

REFERENCES

Aizawa, M., Bluck, B., Cartwright, J.A., Milner, R., Swart, R. & Ward, J. (2000) Constraints on the geomorphological evolution of Namibia from the Offshore Stratigrahic Record. *Commun. Geol. Surv. Namibia*, **12**, 337–346.

Allen, P.A. & Allen, J.R. (1990) *Basin Analysis. Principles and Applications*. Blackwell Scientific Publications, Oxford.

Artemieva, I.M. & Mooney, W.D. (2001) Thermal thickness and evolution of precambrian lithosphere: a global study. *J. Geophys. Res.*, **106**, 16387–16414.

Bauer, K., Neben, S., Schreckenberger, B., Emmermann, R., Hinz, K., Fechner, N., Gohl, K., Schulze, A., Trumbull, R.B. & Weber, K. (2000) Deep structure of the Namibia continental margin as derived from integrated geophysical studies. *J. Geophys. Res.*, **105**, 25829–25853.

Berger, W.H., Lange, C.B. & Wefer, G. (2002) Upwelling history of the Benguela-Namibia System: a synthesis of leg 175 results. In: *Proceedings of the Ocean Drilling Program Leg 175 Scientific Results*, **175** *Benguela Current, Sites 1075–1087* (Ed. by W.H. Berger, G. Wefer & C. Richter), pp. 1–103. National Science Foundation, College Station, TX.

Bolli, H.M., Ryan, W.B.F., Foresman, J.B., Hottmann, W.E., Kagemi, H., Longoria, J.F., Mcknight, B.K., Melguen, M., Natland, J., Proto-decima, F. & Siesser, W.G. (1978) Cape basin continental rise – sites 360 and 361. In: *Initial Reports of the Deep Sea Drilling Project*, **Vol. 40** (Ed. by H.M. Bolli & W.B.F. Ryan, *et al.*) pp. 29–182. U.S. Government Printing Office, Washington.

Bonnet, S. & Crave, A. (2003) Landscape response to climate change: insights from experimental modeling and implications for tectonic versus climatic uplift of topography. *Geology*, **31**, 123–126.

Bray, R., Lawrence, S.R. & Swart, R. (1998) Source rock, maturity data indicate potential off Namibia. *Oil Gas J.*, **96**, 608–614.

Brown, L.F., Benson, J.M., Brink, G.J., Doherty, S., Jollands, A., Jungslager, E.H.A., Keenan, J.H.G., Muntingh, A. & Van Wyk, N.J.S., eds. (1995) *Sequence Stratigraphy in Offshore South African Divergent Basins*, **Vol. 41**. AAPG Studies in Geology, American Association Petroleum Geologists, Tulsa, 184pp.

Brown, R., Summerfield, M.A. & Gleadow, A.J.W. (2002) Denudational history along a transect across the Drakensberg escarpment of Southern Africa derived from apatite fission track thermochronology. *J. Geophys. Res.*, **107**, 2350. doi: 10.1028/2001JB000745

Burke, K. (1996) The African plate. *S. Afric. J. Geol.*, **99**, 341–409.

Burke, K. & Gunnell, Y., eds. (2008) *The African Erosion Surface: A Continental-Scale Synthesis of Geomorphology, Tectonics, and Environmental Change over the Past 180 Million Years* (*Geol. Soc. Am. Memoir*, **201**, 66pp.

Chumakov, N.M., Zharkov, M.A., Herman, A.B., Doludenko, M.P., Kalandadze, N.N., Lebedev, E.L., Ponomarenko, A.G. & Rautian, A.S. (1995) Climatic belts of the Mid-Cretaceous time. *Stratigr. Geol. Corr.*, **3**, 241–260.

Clemson, J., Cartwright, J.A. & Booth, J.R. (1997) Structural segmentation and the influence of basement structure on the Namibian passive margin. *J. Geol. Soc.*, **154**, 477–482.

Clemson, J., Cartwright, J.A. & Swart, R. (1999) The Namib rift: a rift system of possible Karoo age, Offshore Namibia. In: *The Oil and Gas Habitats of South Atlantic* (Ed. by N.R. Cameron, R.H. Bate & V.S. Clure), *Geol. Soc. Spec. Publ. London,* **153**, 381–402.

Clift, P., Gaedick, C., Edwards, R., Lee, J.I., Hildebrand, P., Amjad, S., White, R.S. & Schlüter, H.U. (2002a) The stratigraphic evolution of the Indus fan and the history of sedimentation in the Arabian Sea. *Mar. Geophys. Res.*, **23**, 223–245.

Clift, P., Lee, J.I., Clark, M.K. & Blusztajn, J. (2002b) Erosional response of South China to Arc rifting and Monsoonal strengthening; a record from the South China Sea. *Mari. Geol.*, **184**, 207–226.

Clift, P.D. (2006) Controls on the erosion of Cenozoic Asia and the flux of clastic sediment to the Ocean. *Earth Planet. Sci. Lett.*, **241**, 571–580.

Corner, B., Cartwright, J.A. & Swart, R. (2002) Volcanic passive margin of Namibia: a potential fields perspective. In: *Volcanic Rifted Margins* (Ed. by M. Menzies, S.L. Klemperer, C.J. Ebinger & J. Baker), *Geol. Soc. Am. Spec. Paper,* **362**, 203–220.

Cox, K.G. (1989) The role of mantle plumes in the development of continental drainage patterns. *Nature*, **342**, 873–877.

Deschamps, F., Dauteuil, O., Bourgeois, O., Mocquet, A. & Guillocheau, F. (in press) Post-breakup evolution and palaeotopography of the North Namibian margin during the Meso-Cenozoic. *Tectonophysics*.

de Wit, M. (2007) The Kalahari epeirogeny and climate change: differentiating cause and effect from core to space. *S. Afric. J. Geol.*, **110**, 367–392.

de Wit, M.J., Marshall, T.R. & Partridge, T.C. (2000) Fluvial deposits and drainage evolution. In: *The Cenozoic of Southern Africa* (Ed. by T.C. Partridge & R.R. Maud), *Oxford Monogr. Geol. Geophys.* **40**, 55–72.

Dingle, R.V. & Hendey, Q.B. (1984) Late Mesozoic and tertiary sediment supply to the Eastern Cape Basin (Se Atlantic) and Palaeo-drainage systems in Southwestern Africa. *Mar. Geol.*, **56**, 13–26.

Dingle, R.V., Siesser, W.G. & Newton, A.R. (1983) *Mesozoic and Tertiary Geology of Southern Africa*. Balkema, Rotterdam, 375pp.

Duff, P.M.D. (1993) *Holmes' Principles of Physical Geology.* Chapman & Hall, London, 791pp.

Emery, K.O. & Uchupi, E. (1984) *The Geology of the Atlantic Ocean*. Springer Verlag, Berlin.

Emery, K.O., Uchupi, E., Bowin, C., Phillips, J. & Simpson, E.S.W. (1975) Continental margin off Western Africa: Cape St. Francis (South Africa) to Walvis (South-West Africa). *Am. Assoc. Petrol. Geol. Bull.*, **59**, 3–59.

Exxon World Mapping Project. (1985) *Tectonic Map of the World*. Exxon Production Research Company, Houston, USA.

Fernandez, M., Afonso, J.C. & Ranalli, G. (2010) The deep lithospheric structure of the Namibian volcanic margin. *Tectonophysics*, **481**, 68–81.

Gallagher, K. & Brown, R. (1999a) The Mesozoic Denudation history of the Atlantic margins of Southern Africa and Southeast Brazil and the relationship to offshore sedimentation. In: *The Oil and Gas Habitats of South Atlantic* (Ed. by N.R. Cameron, R.H. Bate & V.S. Clure), *Geological Society Spec Publ. London*, **153**, 41–53.

Gallagher, K. & Brown, R. (1999b) Denudation and uplift at passive margins: the record of the Atlantic margin of Southern Africa. *Philos. Trans. Roy. Soc. London*, **357**, 835–859.

Galloway, W.E. (2001) Cenozoic evolution of sediment accumulation in deltaic and Shore-Zone Depositional Systems, Northern Gulf of Mexico Basin. *Mar. Petrol. Geol.*, **18**, 1031–1040.

Gerrard, I. & Smith, G.C. (1982) Post paleozoic succession and structure of the Southwestern African continental margin. In: *Studies in Continental Margin Geology* (Ed. by J.S. Watkins & C.L. Drake), *Am. Assoc. Petrol. Geol. Mem.*, **34**, 49–74.

Gladczenko, T.P., Hinz, K., Eldhom, O., Meyer, H., Neben, S. & Skogseid, J. (1997) South Atlantic volcanic margins. *J. Geol. Soc.*, **154**, 465–470.

Gladczenko, T.P., Skogseid, J. & Eldhom, O. (1998) Namibia volcanic margin. *Mar. Geophys. Res.*, **20**, 313–341.

Goudie, A.S. (2005) The drainage of Africa since the Cretaceous. *Geomorphology*, **67**, 437–456.

Gurnis, M., Mitrovica, J.X., Ritsema, J. & van Heijst, H. (2000) Constraining mantle density structure using geological evidence of surface uplift rates: the case of the African superplume. *Geochem. Geophys. Geosyst.*, **1**, 1588GC000035.

Hirsch, K.K., Scheck-Wenderoth, M., van Wees, J.-D., Kuhlmann, G. & Paton, D.A. (2010) Tectonic subsidence history and thermal evolution of the orange basin. *Mar. Petrol. Geol.*, **27**, 565–584.

Holtar, E. & Forsberg, A.W. (2000) Postrift development of the Walvis Basin, Namibia: results for the exploration campaign in quadrant 1911. In: *Petroleum Systems of South Atlantic Margins* (Ed. by M.R. Mello & B.J. Katz), *Am. Assoc. Petrol. Geol. Mem.*, **73**, 429–446.

ICS. (2004) International Stratigraphic Chart. International Commission of Stratigraphy. Available at: http://www.stratigraphy.org/.

Jackson, M.P., Cramez, C. & Fonck, J.P. (2000) Role of subaerial volcanic rocks and mantle plume in creation of South Atlantic margins: implications for salt tectonics and source rocks. *Mar. Petrol. Geol.*, **17**, 477–498.

Jones, S.M., White, N.J., Clarke, B.J., Rowley, E. & Gallagher, K. (2002) Present and past influence of the iceland plume on sedimentation. In: *Exhumation of the North Atlantic Margin* (Ed. by A.G. Dore, J.A. Cartwright, M.S. Stocker, J.P. Turner & N.J. White), *Geol. Soc. Spec. Publ. London*, **196**, 13–25.

Kohn, B.P., Gleadow, A.J.W., Brown, R.W., Gallagher, K., Lorencak, M. & Noble, W.P. (2005) Visualizing thermotectonic and denudation histories using apatite fission track thermochronology. *Rev. Mineral. Geochem.*, **58**, 527–565.

Lavier, L.L., Steckler, M.S. & Brigaud, F. (2001) Climatic and tectonic control on the cenozoic evolution of the West African margin. *Mar. Geol.*, **178**, 63–80.

Leturmy, P., Lucazeau, F. & Brigaud, F. (2003) Dynamic interactions between the Gulf of Guinea passive margin and the Congo River drainage basin: 1. Morphology and mass balance. *J. Geophys. Res.*, **108**, 2383–2396.

Light, M.P.R., Maslanyj, M.P., Greenwood, R.J. & Banks, N.L. (1993) Seismic sequence stratigraphy and tectonics offshore Namibia. In: *Tectonics and Seismic Sequence Stratigraphy* (Ed. by G.D. Williams & A. Dobb), *Geol. Soc. Spec. Publ.* **71**, 67–85.

Liu, X. & Galloway, W.E. (1993) Sediment accumulation rate: problems and new approach. In: *Rates of Geologic Processes, Tectonics, Sedimentation, Eustasy and Climate; Implications for Hydrocarbon Exploration* (Ed. by J.M. Armentrout, R. Bloch, H.C. Olson & B.F. Perkins), *GCS-SEPM Foundation 14th Annual Research Conference*, pp. 101–107.

Maslanyj, M.P., Light, M.P.R., Greenwood, R.J. & Banks, N.L. (1992) Extension tectonics offshore Namibia and evidence for passive rifting in the South Atlantic. *Mar. Petrol. Geol.*, **9**, 590–601.

Mcmillan, I.K. (1990) Foraminiferal Biostratigraphy of the Barremian to Miocene Rocks of the Kudu 9a-1, 9a-2 and 9a-3 Boreholes. *Commun. Geol. Survey Namibia*, **6**, 23–29.

Mcmillan, I.K. (2003) Foraminiferally defined biostratigraphic episodes and sedimentation pattern of the cretaceous drift succession (Early Barremian to Late Maastrichian) in seven basins of the South African and Southern Namibian Continental margin. *S. Afric. J. Sci.*, **99**, 537–576.

Melguen, M. (1978) Facies evolution, carbonate dissolution cycles in Sediments from the Eastern South Atlantic (Dsdp Leg 40) since the early cretaceous. In: *Initial Reports of the Deep Sea Drilling Project*, **Vol.40** (Ed. by H.M. Bolli & W.B.F. Ryan, *et al.*) pp. 981–1024. U.S. Government Printing Office, Washington.

Métivier, F. & Gaudemer, Y. (1997) Mass transfer between Eastern Tien Shan and adjacent basins (Central Asia): constraints on regional tectonics and topography (P 1-17). *Geophys. J. Int.*, **128**, 1–253.

Métivier, F. & Gaudemer, Y. (1999) Stability of output fluxes of large rivers in South and East Asia during the last 2 million years: implications on floodplain processes. *Basin Res.*, **11**, 293–303.

Métivier, F., Gaudemer, Y., Tapponier, P. & Meyer, B. (1998) Northeastward growth of the Tibet plateau deduced from balanced reconstruction of two depositional areas: the Qaidam and Hexi Corridor basins, China. *Tectonics*, **17**, 823–842.

Métivier, F., Gaudemer, Y., Tapponnier, P. & Klein, M. (1999) Mass accumulation rates in Asia during the cenozoic. *Geophys. J. Int.*, **137**, 280–318.

Mohriak, W., Rosendahl, B.R., Turner, J.P. & Valente, S.C. (2002) Crustal architecture of South Atlantic volcanic margins. In: *Volcanic Rifted Margins* (Ed. by M. Menzies, S.L. Klemperer, C.J. Ebinger & J. Baker), *Geol. Soc. Am. Spec. Paper*, **362**, 159–202.

Moore, A.E. (1999) A reappraisal of epeirogenic flexure axes in Southern Africa. *S. Afric. J. Geol.*, **102**, 363–376.

Moore, T.C., Rabinowitz, P., Boersma, A., Borella, P.E., Chave, A.D., Duée, D., Fütterer, D.K., Jiang, M.J., Kleinert, K., Lever, A., Manivit, H., S., O.C., Richardson, S.H. & Shackleton, N.J. (1984) *Proceedings of the Deep Sea Drilling Program, Initial Reports*, Washington, 74, 1080pp.

Ni, S., Ding, X., Helmberger, D.V. & Gurnis, M. (1999) Low-velocity structure beneath Africa from forward modeling. *Earth Planet. Sci. Lett.*, **170**, 497–507.

Ni, S., Tan, E., Gurnis, M. & Helmberger, D. (2002) Sharp sides to the African superplume. *Science*, **296**, 1850–1852.

Nyblade, A.A., Owens, T.J., Gurrola, H., Ritsema, J. & Langston, C.A. (2000) Seismic evidence for a deep upper mantle thermal anomaly beneath East Africa. *Geology*, **28**, 599–602.

Nyblade, A.A. & Robinson, S.W. (1994) The African superswell. *Geophys. Res. Lett.*, **21**, 765–768.

Nyblade, A.A. & Sleep, N.H. (2003) Long lasting epeirogenic uplift mantle plumes and the origin of the Southern African plateau. *Geochem. Geophys. Geosyst.*, **4**, 1105, doi 1110.1029/2003GC0000573.

Partridge, T.C. & Maud, R.R. (1987) Geomorphic evolution of Southern Africa since the mesozoic. *S. Afric. J. Geol.*, **90**, 179–208.

Paton, D.A., di Primio, R., Kuhlmann, G., van der Spuy, D. & Horsfield, B. (2007) Insights into the petroleum system evolution of the Southern Orange Basin, South Africa. *S. Afric. J. Geol.*, **110**, 261–274.

Paton, D., van der Spuy, D., di Primio, R. & Horsfield, B. (2008) Tectonically induced adjustment of passive margin accommodation space; influence on the hydrocarbon potential of the Orange Basin, South Africa. *Am. Assoc. Petrol. Geol. Bull.*, **92**, 589–609.

Pickford, M., Senut, B., Mein, P., Gommery, D., Morales, J., Soria, D., Nieto, M. & Ward, J. (1996) Preliminary results of new excavations at Arrisdrift, Middle Miocene of Southern Namibia. *C. R. Acad. Sci. Paris*, **322**, 991–996.

Poag, C.W. & Sevon, W.D. (1989) A record of Appalachian denudation in Post-Rift Mesozoic and Cenozoic sedimentary deposits of the U.S. Middle Atlantic Continental margin. *Geomorphology*, **2**, 119–157.

Pysklywec, R.N. & Mitrovica, J.X. (1999) The role of subduction induced subsidence in the evolution of the Karoo basin. *J. Geol.*, **107**, 155–164.

Raab, M.J., Brown, R.W., Gallagher, K., Carter, A. & Weber, K. (2002) Late Cretaceous reactivation of major crustal shear zones in Northern Namibia: constraints from Apatite Fission Track Analysis. *Tectonophysics*, **349**, 75–92.

Raab, M.J., Brown, R.W., Gallagher, K., Weber, K. & Gleadow, A.J.W. (2005) Denudational and thermal history of the early cretaceous Brandberg and Okenyenya igneous complexes on Namibia's Atlantic passive margin. *Tectonics*, **24**, TC3006, doi:3010.1029/2004TC001688.

Rayner, R.J., Waters, S.B., Mckay, I.J., Dobbs, P.N. & Shaw, A.L. (1991) The mid-cretaceous palaeoenvironment of Central Southern Africa (Orapa, Botswana). *Palaeogeogr. Palaeoclimatol. Palaeoecol.*, **88**, 147–156.

Ritsema, J. & van Heijst, H. (2000) New seismic model of the upper mantle beneath Africa. *Geology*, **28**, 63–66.

Ritsema, J., van Heijst, H. & woodhouse, J. (1999) Complex shear wave velocity structure imaged beneath Africa and Iceland. *Science*, **286**, 1925–1928.

Rouby, D., Bonnet, S., Guillocheau, F., Gallagher, K., Robin, C., Biancotto, F., Dauteuil, O. & Braun, J. (2009) Sediment supply to the orange sedimentary system over the last 150 My: an evaluation from sedimentation/denudation balance. *Mar. Petrol. Geol.*, **26**, 782–794.

Rust, D.J. & Summerfield, M.A. (1990) Isopach and borehole data as indicators of rifted margin evolution in Southwestern Africa. *Mar. Petrol. Geol.*, **7**, 277–287.

Scholtz, A. (1985) The palynology of the upper lacustrine sediments of the Arnot Pipe, Banke, Namaqualand. *Ann. S. Afr. Museum*, **95**, 1–109.

Sclater, J.G. & Christie, P.A.F. (1980) Continental stretching: an explanation of the mid-cretaceous subsidence of the Central North Sea basin. *J. Geophys. Res.*, **85**, 3711–3739.

Ségalen, L., Renard, M., Pickford, M., Senut, B., Cojan, I., Le Callonnec, L. & Rognon, P. (2002) Environmental and climatic evolution of the Namib Desert since the Middle Miocene: the contribution of carbon isotope ratios in Ratite Eggshells. *C. R. Geosci.*, **334**, 917–924.

Ségalen, L., Rognon, P., Pickford, M., Senut, B., Emmanuel, L., Renard, M. & Ward, J. (2004) Reconstitution of dune morphologies and palaeowind regimes in the Proto-Namib since the Miocene. *Bull. Soc. Géol. France*, **175**, 537–546.

Selby, M.J. (1985) *Earth's Changing Surface: An Introduction to Geomorphology*. Clarendon Press, Oxford, 602pp.

Senut, B., Pickford, M. & Ségalen, L. (2009) Neogene desertification of Africa. *C. R. Geosci.*, **341**, 591–602.

Siesser, W.G. (1980) Late miocene origin of the Benguela upwelling system off Northern Namibia. *Science*, **208**, 283–285.

Smith, R.M.H. (1986) Sedimentation and palaeoenvironments of late cretaceous crater-lake deposits in Bushmanland, South Africa. *Sedimentology*, **33**, 369–386.

Smith, W.H.F. & Sandwell, D.T. (1997) Global seafloor topography from satellite altimetry and ship depth soundings. *Science*, **277**, 1957–1962.

Stevenson, I.R. & Mcmillan, I.K. (2004) Incised valley fill stratigraphy of the upper cretaceous succession, proximal orange basin, Atlantic margin of Southern Africa. *J. Geol. Soc.*, **161**, 185–208.

Tinker, J., de Wit, M. & Brown, R. (2008a) Mesozoic exhumation of the Southern Cape, South Africa, quantified using apatite fission track thermochronology. *Tectonophysics*, **455**, 77–93.

Tinker, J., de Wit, M. & Brown, R. (2008b) Linking source and sink: evaluating the balance between onshore erosion and offshore sediment accumulation since Gondwana Break-up, South Africa. *Tectonophysics*, **455**, 94–103.

Trumbull, R.B., Sobolev, S.V. & Bauer, K. (2002) Petrophysical modeling of high seimic velocity crust at the Namibian Volcanic margin. In: *Volcanic Rifted Margins* (Ed. by M. Menzies, S.L. Klemperer, C.J. Ebinger & J. Baker), *Geol. Soc. Am. Spec. Paper*, **362**, 221–230.

Tucholke, B.E. & Embley, R.W. (1984) Cenozoic regional erosion of the Abyssal sea floor off South Africa. In: *Interregional Unconformities and Hydrocabon Accumulation* (Ed. by J.S. Schlee), *Am. Assoc. Petrol. Geol. Mem.*, **36**, 145–164.

Uenzelmann-Neben, G., Schluter, P. & Weigelt, E. (2007) Cenozoic oceanic circulation within the South African gateway: indications from seismic stratigraphy. *S. Afric. J. Geol.*, **110**, 275–294.

UNESCO, Choubert, G. & Faure-Muret, A. (1990) International Geological Map of Africa, CGWM & UNESCO.

van der Beek, P., Summerfield, M.A., Braun, J., Brown, R.W. & Fleming, A. (2002) Modeling postbreakup landscape development and denudational history of the Southeast African (Drakensberg Escarpment) margin. *J. Geophys. Res.*, **107**, 2351.

van der Spuy, D. (2003) Aptian source rocks in some South African Cretaceous basins. In: *Petroleum Geology of Africa: New Themes and Developing Technologie* (Ed. by M.A. Arthur, D.S. MacGregor & N.R. Cameron), *Geol. Soc. Spec. Publ. London*, **207**, 185–202.

Walford, H.L., White, N.J. & Sydow, J.C. (2005) Solid sediment load history of the Zambezi delta. *Earth Planet. Sci. Lett.*, **238**, 49–63.

Wefer, G., Berger, W.H., Richter, C., Adams, D.D., Anderson, L.D., Andreasen, D.J., Brüchert, V., Cambray, H., Christensen, B.A., Frost, G.M., Giraudeau, J., Gorgas, T.J., Hermelin, J.O.R., Jansen, J.H.F., Lange, C.B., Laser, B., Lin, H.L., Maslin, M.A., Meyers, P.A., Motoyama, I., Murray, R.W., Perez, M.E., Pufahl, P.K., Spiess, V., Vidal, L., Wigley, R., & Yamazaki, T. (1998) *Proceedings of the Ocean Drilling Program, Initial Reports*, 175, 577pp.

Wickens, H.D.V. & Mclachlan, I.R. (1990) The stratigraphy and sedimentology of the reservoir interval of the Kudu 9a-2 and 9a-3 boreholes. *Commun. Geol. Surv. Namibia*, **6**, 9–22.

Manuscript received 29 January 2010; Manuscript accepted 18 April 2011.